




ORIGINAL ARTICLE

Food Restriction Engages Prefrontal Corticostriatal Cells and Local Microcircuitry to Drive the Decision to Run versus Conserve Energy

Adrienne N. Santiago ¹, Emily A. Makowicz ^{1,2}, Muzi Du^{1,3} and Chiye Aoki ^{1,4}

¹Center for Neural Science, New York University, 4 Washington place, New York, NY 10003, USA, ²Hunter College, City University of New York, 695 Park Ave, New York, NY, 10065, USA, ³Langone Neuroscience Institute, New York University, 435 East 30th St, New York, NY 10016, USA and ⁴New York University Shanghai, 1555 Century Ave, Pudong, Shanghai 200122, China

Address correspondence to Adrienne N. Santiago, Center for Neural Science, New York University, 4 Washington place, New York, NY 10003, USA. Tel: 917-586-9227; Fax: 212-995-4011; Email: ans525@nyu.edu.

Abstract

Food restriction (FR) evokes running, which may promote adaptive foraging in times of food scarcity, but can become lethal if energy expenditure exceeds caloric availability. Here, we demonstrate that chemogenetic activation of either the general medial prefrontal cortex (mPFC) pyramidal cell population, or the subpopulation projecting to dorsal striatum (DS) drives running specifically during hours preceding limited food availability, and not during *ad libitum* food availability. Conversely, suppression of mPFC pyramidal cells generally, or targeting mPFC-to-DS cells, reduced wheel running specifically during FR and not during *ad libitum* food access. Post mortem c-Fos analysis and electron microscopy of mPFC layer 5 revealed distinguishing characteristics of mPFC-to-DS cells, when compared to neighboring non-DS-projecting pyramidal cells: 1) greater recruitment of GABAergic activity and 2) less axo-somatic GABAergic innervation. Together, these attributes position the mPFC-to-DS subset of pyramidal cells to dominate mPFC excitatory outflow, particularly during FR, revealing a specific and causal role for mPFC-to-DS control of the decision to run during food scarcity. Individual differences in GABAergic activity correlate with running response to further support this interpretation. FR enhancement of PFC-to-DS activity may influence neural circuits both in studies using FR to motivate animal behavior and in human conditions hallmarked by FR.

Key words: anorexia, DREADD, GABA, prefrontal cortex, striatum

Introduction

Adaptive behavioral modification in times of food scarcity can provide individuals with an evolutionary advantage. In many diverse species, food restriction (FR) evokes an increase in running, which promotes adaptive foraging behaviors (de Lartigue and McDougle 2019; Södersten et al. 2019). Although running to seek new locations with potentially greater resources may be adaptive in some circumstances, FR-evoked running is potentially life threatening, if energy expenditure exceeds caloric availability. In adolescent mice, restriction of food to a 2-hour

window is nonlethal (Chowdhury et al. 2013; Chen et al. 2018a), yet when given access to a running wheel, as in the activity-based anorexia (ABA) model (Gutierrez 2013), FR mice can lose between 20 and 25% body weight in as little as 3 days, increasing risk for mortality (Chowdhury et al. 2013). The greatest increase in excessive running occurs during the hours leading up to the scheduled feeding time (food anticipatory activity [FAA]) (Mistlberger 2020). The extent of FR-evoked running is hallmarked by variance, and individual differences in running responses correlate with an increase in anxiety-like behavior (Wable et al.

2015). Despite the prevalence of FR as a tool to motivate animal behavior (Goltstein et al. 2018), little is known about the neural pathways that drive FR-evoked hyperactivity.

In dorsal striatum (DS), where dopamine signals a feeding-entrained oscillator (de Lartigue and McDougale 2019), FAA requires expression of dopamine D1 receptors (D1R) (Gallardo et al. 2014). Striatal D1R cells are the major players in the direct pathway to initiate movement (Gerfen and Surmeier 2011). FR increases DS sensitivity to D1R-mediated dopaminergic activity (Carr 2002). The pleasurable act of voluntary wheel running (Meijer and Robbers 2014) also induces a hyperdopaminergic state in DS, wherein even aversive stimuli, such as an energy-depleted state, can activate circuitry of reward and addiction (Kanarek et al. 2009; Greenwood 2019). This positions DS as a likely target for executing FR-evoked running. The question remains: Is top-down control of DS-mediated running FR-dependent?

One major excitatory input to the DS, the medial prefrontal cortex (mPFC), has not as of yet been causally implicated in generating FR-evoked running. FR shifts circadian c-Fos expression in the mPFC to produce a spike in activity corresponding to FAA (Angeles-Castellanos et al. 2007). mPFC c-Fos levels also increase during states of food reward expectation (Valdes et al. 2006). Temporal control of goal-directed behavior requires mPFC pyramidal cells expressing D1R (Narayanan et al. 2012), a cell type known to project from layer 5 of mPFC to DS (Anastasiades et al. 2019). We therefore used multiplexed chemogenetics to test the prediction that FR gates mPFC pyramidal cell control of hyperactive running. Specifically, we determined whether activation and suppression of these cells modulates FR-evoked running without altering running under *ad libitum* food. We further tested whether modulation of mPFC-to-DS-projecting pyramidal cells is sufficient or requires additional mPFC pyramidal cells with diverse projections to modulate FAA running.

How does microcircuitry of the mPFC contribute to FR-evoked running? mPFC parvalbumin-positive GABAergic interneurons (GABA-INs) increase firing during goal-directed behavior (Kim et al. 2016) and express D1R (Anastasiades et al. 2019). Likewise, the lateral hypothalamus, which registers and engages responses to FR and other aspects of homeostasis (Stuber and Wise 2016), projects directly to mPFC GABA-INs (Stuber et al. 2011). Moreover, lengths of GABAergic axon terminals targeting mPFC pyramidal cells correlate negatively with FR-evoked running (Chen et al. 2016), suggesting that mPFC GABA-INs may dampen FR-evoked running. Here, we ask whether the extent of mPFC pyramidal cell recruitment of GABA-INs contributes to individual differences in FR-evoked running. To this end, we quantified the extent of c-Fos expression in GABA-INs following excitation of mPFC pyramidal cells. We then used electron microscopy to ask whether GABA-INs target the mPFC-DS subpopulation and non-DS-projecting pyramidal cells equally, or skews to favor one subpopulation. Our findings led us to a new interpretation of the role of GABA-INs in facilitating mPFC-to-DS pyramidal cells to drive running specifically during FR.

Methods

Experimental Design

Additional details for methods regarding subjects, stereotaxic surgery, drug dosage, brain tissue preparation, and immunohistochemistry are available in [Supplemental Materials](#). Because of

the prevalence of anorexia nervosa (AN) in adolescent females (Murray et al. 2017), and the relevance of this work to researchers studying that disorder, only adolescent female C57/BL6 mice were used for this study. Adolescent rodents are also more susceptible to FR-evoked running, versus adults (Gelegen et al. 2006; Gilman et al. 2019), which parallels the common adolescent onset of AN in the human population (Herpertz-Dahlmann 2015).

For all studies, mice were assigned randomly to receive injection of either control virus or viruses for transcription of Designer Receptors Exclusively Activated by Designer Drugs (DREADDs) before any measure of activity was collected. Power analysis was conducted to estimate the sample size needed.

To drive both cell firing and cell suppression within the same target population, we simultaneously injected two DREADD viruses into a single mouse, with the hM3D(Gq) receptor to activate cell firing and the kappa-opioid DREADD (KORD) receptor to suppress cell firing. Because the Gq receptor ligand CNO can reverse-metabolize to clozapine to produce off-target effects (Gomez et al. 2017), we chose to use the C21 ligand, which has been extensively characterized to show minimal off-target agonist activity at the dosage we used (1 mg/kg) (Thompson et al. 2018). The KORD receptor ligand, Salvinorin B (SalB) has also been characterized extensively to be pharmacologically inert except as agonist to KORD (Vardy et al. 2015; Marchant et al. 2016). To target mPFC pyramidal cells, we injected DREADD viruses under a CaMKII α promoter into the mPFC (CaMKII group; Fig. 1A). To target the mPFC-DS pathway, we injected cre-dependent DREADDs into the mPFC and a retrograde cre virus into the DS (mPFC-DS group; Fig. 1A). mPFC-DS and CaMKII group experiments were run concurrently.

Littermates of mPFC-DS and CaMKII subjects were used as control subjects for both experimental groups. Three different types of control subjects were used, all lacking expression of DREADD genes (Fig. 1A). CaMKII α -GFP control group “GFP-CON” mice ($N=5$) were injected with CaMKII α -GFP virus into the mPFC. This group controlled for energy expenditure required to replicate the virus in pyramidal cells of the mPFC. “No-cre-CON” subjects ($N=6$) were injected with cre-dependent DREADD virus in the mPFC without injection of the retrogradely transported cre-virus. This control was used to ensure that the cre-dependence of the cre-dependent DREADDs was functional, and was validated based on the finding that neither DREADD reporter was transcribed for these controls. Both the GFP-CON and No-cre-CON groups, ($N=11$, collectively) received DREADD ligand administration that was identical to that of experimental DREADD mice, and were perfused alongside mice from the CaMKII and mPFC-DS experimental groups. A third control group, “No-Drug-cre-CON” subjects ($N=5$), were injected with GFP-cre virus into a control region, the dorsal hippocampus, to control for surgical experience and energy expenditure required to replicate cre virus within the brain. In contrast to the other control groups, the No-Drug-cre-CON subjects did not receive DREADD ligand, so as to provide a control to assess whether drug administration in the absence of DREADD receptor would perturb behavior. These mice were perfused immediately after the end of the second round of FR. We detected no significant differences between control groups (see Results section) for any of the variables we observed in this report. Therefore, data for all three types of control were pooled under the “CON” group ($N=15$). This CON group was used as comparison for all data points collected from the first introduction of the wheel to the

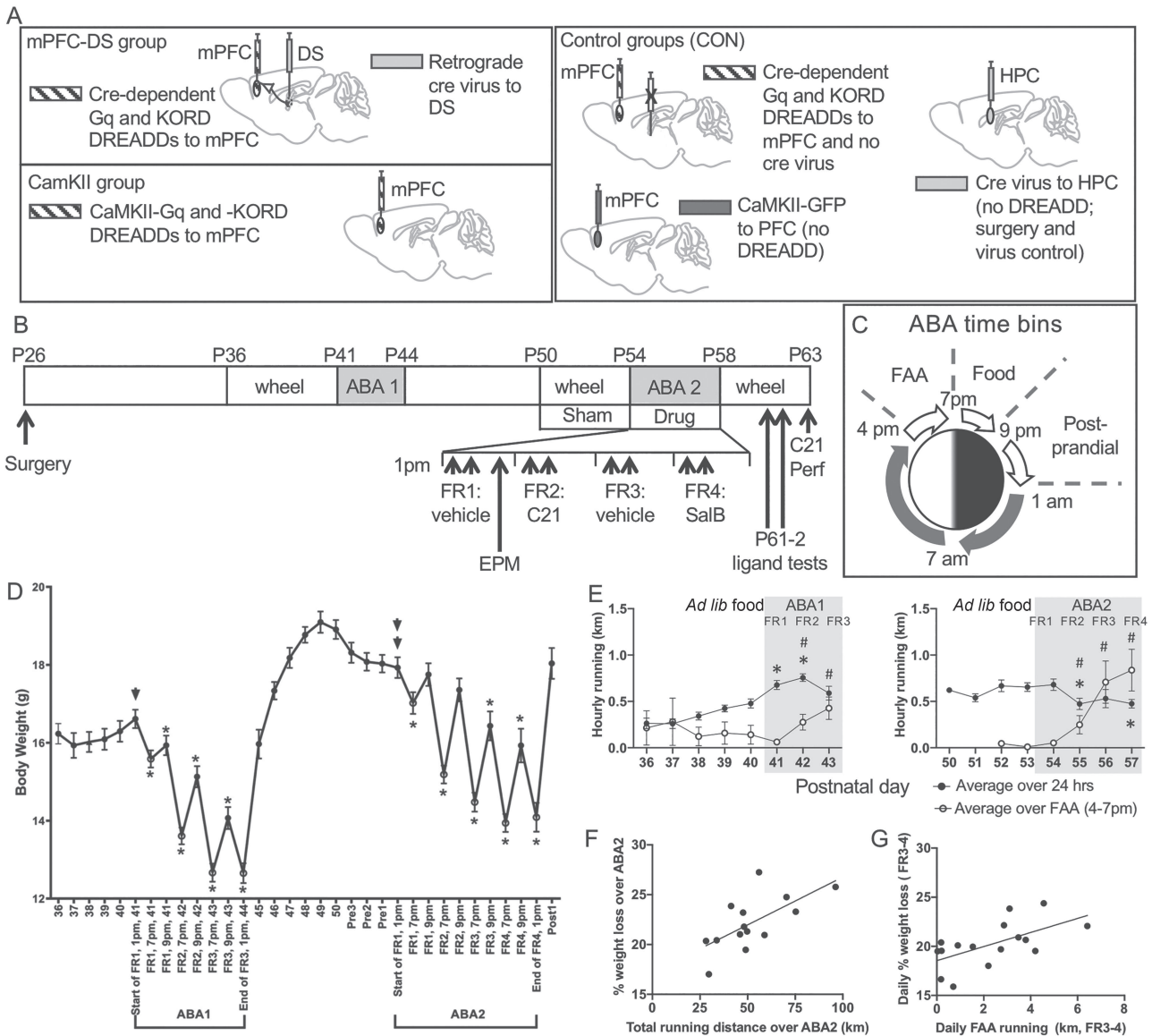


Figure 1. Experimental design and changes in body weight and wheel running evoked by ABA induction. **A.** Experimental groups consisted of 1) the mPFC-DS group, where cre-dependent Gq and KORD DREADDs were injected into the mPFC and retrograde cre virus was injected into the DS. This enabled selective DREADD expression in the subset of mPFC pyramidal cells that project to DS. 2) CamKII group where viral transcription for Gq and KORD DREADDs was under control of a CamKII α promoter and delivered into the mPFC to target mPFC pyramidal cells. The control (CON) group consisted of three subgroups: 1) “no-CRE-CON” (N=6) were injected with cre-dependent DREADD virus in the mPFC without injection of the retrogradely transported cre-virus, thus ensuring that the cre-dependence of the DREADDs was functional 2) “GFP-CON” (N=5) were injected with CamKII α -GFP virus into the mPFC for GFP expression selectively in mPFC pyramidal cells 3) “No-Drug-cre-CON” subjects (N=5), were injected with GFP-cre virus into a control region, the dorsal hippocampus (HPC), and unlike the other 11 control subjects, they did not receive DREADD ligand to test for off-target effects of the ligand **B.** ABA induction schedule. All animals underwent viral injection surgery at or around postnatal day 26 (P26). After surgery, mice were singly housed. On P36 \pm 1, a wheel was introduced to the cage and baseline wheel running and weight measures were recorded. The first bout of ABA (ABA1) began at 1 pm on P41, at which time food was removed, but the wheel was left in cage. For a total of 3 days, food access was restricted to the hours of 7 pm to 9 pm, corresponding to the beginning of the dark phase of the light-dark cycle. At 1 pm on P44 \pm 1, FR of ABA1 was terminated: wheels were removed and food access was *ad libitum*. Following up to 6 days of recovery, wheel reacclimation began, followed by 4 days of baseline wheel running measurements. The second bout of ABA (ABA2) began at 1 pm, whereby food was removed at all hours except for 7 pm to 9 pm. Of the 4 food restricted days (FR1 through 4), the ligand, C21 for Gq-DREADD was injected on FR2 and the ligand, Salvinorin B (SalB) for KORD was injected on FR4, with vehicle injected on FR1 and FR3. Following 4 days of FR, food access returned to be *ad libitum* and wheel was available, so as to measure DREADD ligand modulation of wheel activity in the absence of FR. Following these ligand tests during recovery, animals were injected with either C21 or SalB, then euthanized approximately 2 h later by transcardial perfusion under urethane anesthesia for retrospective analysis of neuronal activation based on c-Fos-immunoreactivity and for electron microscopic analyses. **C.** Schematic of the three time bins measured daily during FR and recovery: FAA (4–7 pm), food allowance period (food, 7–9 pm), and the postprandial period (9 pm–1 am). **D.** Body weights across the days preceding, during and following ABA inductions of control (CON) mice. Single arrow points to the baseline value at the start of FR1 of ABA1, at 1 pm on P41. Double arrow points to the baseline body weight at the start of FR1 of ABA2. Asterisks indicate body weights that were significantly less than the baseline value. Values are mean \pm SEM. **E.** Hourly wheel running of CON mice during the days preceding and during ABA. Filled circle: hourly wheel running distance averaged over the course of the 24 h/day; asterisk indicates significant difference versus measure from day prior to FR induction. Open circle: hourly wheel running distance averaged over the 3 h FAA time bin (4–7 pm); hashtag indicates significant difference versus measure from FR1, which occurs 3 h following FR induction. Note the precipitous rise of FAA during ABA1 and ABA2. **F.** Total running over the 4 days of ABA2 correlated positively with percent weight loss over the same timeframe ($P = 0.010$, $R = 0.66$). **G.** FAA running, averaged over FR3 and FR4, correlated positively with daily percent weight loss averaged over the same period ($P = 0.014$, $R = 0.602$).

end of the second bout of FR. For data points collected during recovery from the second bout of FR, only the mice from the GFP-CON and No-cre-CON groups were used, as the No-Drug-cre-CON subjects were perfused immediately following the second bout of FR.

Fifteen subjects were used for the CaMKII group. Of these, eight received C21 on the second day of FR (FR2) and 10 received SalB on the fourth day of FR (FR4), with three mice receiving both C21 on FR2 and SalB on FR4. For the mPFC-DS group, all nine mice received C21 to activate cell firing on FR2 and received SalB to suppress cell firing on FR 4. Our wheel hub malfunctioned on FR2 for one cohort consisting of two “no-cre CON” (described below) and two mPFC-DS mice. This warranted exclusion of data from time-bins overlapping with the outage, but not exclusion of data at points when the hub was functioning. Otherwise, exclusion criteria were limited to death, abnormal locomotion on the elevated plus maze (administered before DREADD ligand drug administration), and insufficient bilateral viral replication in the region of interest (two animals, with one each from the CaMKII and mPFC-DS groups).

Human bias was limited by masking group identity to keep the experimenter blind to experimental condition during all feeding, weight measurement, and drug/vehicle administration procedures. Wheel count was automatized, and analysis of immunofluorescent images, used to assess DREADD modulation of neurons, was also performed blind to experimental condition.

ABA Induction

Because AN commonly has adolescent onset and a relapsing course (Wentz et al. 2009), all mice (both control and experimental) underwent two bouts of ABA (FR plus wheel access), timed during mid and late adolescence (Fig. 1B), as previously described (Chen et al. 2016; Chen et al. 2018b). At $P36 \pm 1$, mice were provided with unlimited access to a running wheel capable of collecting continuous wheel count data (2654.86 turns per kilometer; Med Associates, Fairfax, VT). Following 5 days of acclimation, animals underwent a first bout of FR (ABA1), which lasted 3 days. During this time, food was restricted to a 2-hour period from 7 pm to 9 pm each night, unlimited in amount, while wheel access remained unlimited (Fig. 1C). After the third day of FR, the wheels were removed for a 4-day recovery period. On $P50 \pm 1$, the wheels were replaced for 4 days of re-acclimation, after which the mice were subjected to a second bout of ABA lasting 4 days (ABA2). Afterwards, mice remained with unlimited wheel and food access until euthanasia by transcardial perfusion, 5 days later. One exception was of the 5 “No-Drug-cre-CON” mice that were perfused at the end of ABA2, rather than euthanizing them 5 days after the end of ABA2.

Drug Delivery

Subcutaneous injection of C21 was delivered on FR2, SalB was delivered on FR4, and vehicle was delivered on FR1 and FR3. On each of the 4 days leading up to FR1, mice were given a sham injection (no needle insertion) to climatize mice to the stress of brief restraint. Because C21 drug activity (Chen et al. 2015; Thompson et al. 2018) lasts longer than that of SalB (Vardy et al. 2015), drug delivery times were staggered, aiming to target the hours of FAA and food availability. For the CaMKII experiment, C21 was delivered at 12 noon and 6:00 pm, while SalB was

delivered at 3:30 and 6:30 pm. For the mPFC-DS group, C21 was delivered at 3:30 and 9:30 pm, while SalB was delivered at 3:30 and 6:30 pm. Drug was delivered on day 2 and/or 4 of ABA2 (Fig. 1B). Drugs were also delivered on postrecovery days, to test the effects of cell activation/suppression in the context of *ad libitum* food availability (Fig. 1B). Additionally, either C21 or SalB was delivered ~2 h before perfusion, so as to reveal the extent of drug-induced cell activity/suppression by immunohistochemical detection of c-Fos protein within the virally infected portion of mPFC.

EM Analysis

EM analysis was performed only on mPFC-DS group subjects that received C21 injection prior to perfusion ($N=7$). Layer 5 pyramidal cells, identified by a smooth nuclear envelope and lack of GAD+ immunolabeling, were categorized as either DS-projecting (mCherry+) or non-DS-projecting (mCherry-). For each subject, 10 mCherry+ and 10 mCherry- pyramidal cells were quantified. For each cell, percent GABAergic innervation was calculated as the summed length of somatic plasma membrane contacted by GAD+ terminals over the perimeter of the somatic plasma membrane for that cell profile. Density of GABAergic innervation was calculated as the number of GABAergic terminals contacting a cell soma over the perimeter length of the somatic plasma membrane profile. Each of the 10-cell measurements for a single subject were averaged together before performance of a t-test.

Statistical Analyses

For data assessing two experimental groups (CON vs. CaMKII or CON vs. mPFC-DS), an F test was performed to establish whether standard deviations (SDs) were significantly different between groups. If SDs were not significantly different ($P > 0.05$), an unpaired, two-tailed t-test was performed. If SDs were significantly different ($P < 0.05$), an unpaired, two-tailed t-test with Welch's correction was performed. Statistical analysis was performed and graphs were produced using the software Prism v. 6 or v. 8 (GraphPad Software, Inc.).

Our primary experimental design for analysis of running behavior uses a Planned Comparison to test DREADD effects on three time bins (FAA; 2-h food availability; postprandial periods), with a hypothesis that engaging DREADD receptors would affect running specifically during the FAA period. This is the primary report in the Results section. Because each of the three time bins is a different length of time (3, 2, 4 h, respectively) we included Complementary comparisons within each bin to describe hour-by-hour changes. Because mathematical corrections for multiple comparisons are not generally recommended for these types of planned and complementary comparisons (Rothman 1990), we report only uncorrected t-tests for all between-group comparisons of hour-bin data. Correlation data were assessed by simple linear regression, and Pearson R values and P values were reported.

Results

ABA Induction of CON Mice Reveals Daily Increase in FAA.

As described in the methods, three different subgroups were used for CON mice: “GFP-CON” mice ($N=5$; injected with CaMKII-GFP virus into the mPFC), “No-cre-CON” ($N=6$; viral

injection of cre-dependent DREADDs but no cre virus), and “No-Drug-cre-CON” ($N=5$; viral injection of cre-eGFP virus and no DREADD or drug delivery). There were no significant differences between any of the CON subgroups, either in weight loss or running distance or duration, neither during FAA (4–7 pm) nor food availability (7–9 pm).

During ABA1, CON mice lost body weight significantly as compared to baseline, defined as the measure taken immediately prior to the start of ABA1 at 1 pm., and mice were unable to regain body weight during the 2 h of food availability (Fig. 1D). During ABA2, CON mice likewise lost body weight significantly due to restricted food access. Unlike during ABA1, mice during ABA2 were able to regain body weight to baseline levels by the end of the 2 h of food access of FR day1 and 2 (FR1, 9 pm; FR2, 9 pm in Fig. 1D) but not during FR3 or FR4.

During ABA1, CON mice significantly increased their hourly wheel running distance, averaged over the course of the day, with a 41.5% increase above baseline during FR1 ($t(30)=2.414$, $P=0.022$, unpaired t-test) and a 58.0% increase above baseline during FR2 ($t(30)=2.614$, $P=0.014$, unpaired t-test), but which subsequently declined to a level no longer different from baseline by FR3 ($t(30)=1.463$, $P=0.154$, unpaired t-test; Fig. 1E). By contrast, hourly running distance averaged over the course of the 3 h of FAA (4–7 pm) increased steadily throughout ABA1. Because FR is imposed at 1 pm, the 4–7 pm FAA on FR1 occurred after only 3 h of daylight FR. As expected, this extent of FR did not evoke any significant change in behavior. However, by FR2, the average hourly FAA running had increased by 341% above FR1 ($t(18.2)=2.360$, $P=0.030$, Welch's t-test; Fig. 1E), and by FR3, percent increase was up to 584% above FR1 ($t(16.1)=2.923$, $P=0.010$, Welch's t-test).

During ABA2, hourly running distance of CON mice, averaged over the course of the day, did not increase, unlike what was observed during ABA1. Instead, there was a significant decrease of 27.7% on FR2 ($t(28)=2.40$, $P=0.023$, unpaired t-test) and 27.3% on FR4 ($t(30)=2.73$, $P=0.011$, unpaired t-test), versus baseline (Fig. 1E). By contrast, hourly running distance averaged over the course of FAA, increased robustly throughout ABA2—by 1258% on FR3 ($t(15.46)=2.864$, $P=0.012$, Welch's t-test) and by 1505% on FR4 ($t(15.47)=3.452$, $P=0.003$, Welch's t-test), versus FR1. Total running over the 4 days of ABA2 correlated positively with percent weight loss over the same timeframe ($P=0.010$, $R=0.661$, Fig. 1F), indicating that high runners were the most at risk for precipitous weight loss. Note that FR3 and FR4 were the days when hourly FAA exceeded the hourly running averaged over the course of the day. On these days, the average daily FAA running correlated positively with daily percent weight loss ($P=0.014$, $R=0.602$, Fig. 1G). By contrast, daily postprandial running (9 pm–1 am, Fig. 1C) over FR3–4 did not correlate with daily percent weight loss ($P=0.361$, $R=0.245$).

The increase in FAA over the course of FR is not a novel finding (Chowdhury et al. 2013), but the role of PFC pyramidal neurons in FAA remained unknown. To test the hypothesis that these pyramidal neurons evoke FAA, we used C21 to activate Gq-DREADD expressed by PFC pyramidal neurons on FR2, when FAA running is relatively lower, and suppressed cell firing on FR4 using SalB KORD-DREADD, when FAA running is relatively higher, so as to minimize ceiling and floor effects that could obscure DREADD ligand effects.

C21/Gq-DREADD Activation of the Subset of mPFC Pyramidal Cells Projecting to DS Increases FR-Evoked Running during FAA

For the mPFC-DS group, delivery of C21 during FAA of FR2 (4–7 pm) significantly increased running distance by 245% versus CON subjects ($t(19)=3.085$, $P=0.006$, unpaired t-test), with significant between-group differences during the hour bins of 4–5 pm ($t(19)=2.117$, $P=0.048$, unpaired t-test) and 5–6 pm ($t(19)=4.006$, $P<0.001$, unpaired t-test). Running duration over the 4–7 pm FAA period also increased by 194% ($t(19)=3.206$, $P=0.010$, unpaired t-test), compared to CON subjects (Fig. 2A). By contrast, delivery of C21 to the same mice during the same temporal period but after body weight restoration had no effect on running distance ($t(14)=0.705$, $P=0.492$, unpaired t-test) or running duration ($t(14)=0.202$, $P=0.843$, unpaired t-test; Fig. 2B). Thus, C21 delivery specifically increases FAA running during FR, but has no effect on running in general, when food is freely available. DREADD-driven effects observed during FAA of FR2 were no longer present during FAA of FR3, 18 h after the last ligand delivery (vs. CON; for distance: $t(23)=1.208$, $P=0.239$, unpaired t-test; for duration: $t(23)=1.097$, $P=0.284$, unpaired t-test).

As previously reported (Chen et al. 2018a), running distance and duration decreased dramatically for all animals following transition from FAA hours to feeding time (7–9 pm). Delivery of C21 on FR2 had no further effect on feeding time (7–9 pm), running distance ($t(19)=0.508$, $P=0.617$, unpaired t-test) or duration ($t(7.694)=0.540$, $P=0.604$, Welch's t-test; Fig. 2A), compared to CON subjects. Likewise, delivery of C21 to the same animals during the same hours but after weight restoration had no effect on running distance ($t(14)=0.133$, $P=0.896$, unpaired t-test) or running duration ($t(14)=0.126$, $P=0.901$, unpaired t-test; Fig. 2B).

Delivery of C21 on FR2 had no effect on postprandial (9 pm–1 am) running distance ($t(19)=1.170$, $P=0.257$, unpaired t-test) or duration ($t(7.321)=1.181$, $P=0.274$, Welch's t-test; Fig. 2A), relative to CON subjects' postprandial running. Likewise, delivery of C21 to the same animals after weight restoration had no effect on 9 pm–1 am running distance ($t(14)=0.747$, $P=0.467$, unpaired t-test) or running duration ($t(14)=0.529$, $P=0.605$, unpaired t-test; Fig. 2B). Thus, selective activation of DS-projecting mPFC cells increases FAA running without affecting subsequent running during the 2 h of food availability or the postprandial period.

SalB/KORD Suppression of the Subset of mPFC Pyramidal Cells Projecting to DS Reduces FR-Evoked Running

Delivery of SalB on FR4 significantly decreased running distance during FAA (4–7 pm) by 71.6% ($t(20.04)=2.427$, $P=0.025$, Welch's t-test; Fig. 2C), with a significant decrease at the 6–7 pm time bin immediately preceding food availability ($t(23)=2.944$, $P=0.007$, unpaired t-test). Likewise, running duration decreased by 58.5% ($t(22.15)=2.204$, $P=0.038$, Welch's t-test). By contrast, delivery of SalB in recovered mice during the same hours had no effect on running distance ($t(17)=0.124$, $P=0.231$, unpaired t-test) or duration ($t(17)=0.697$, $P=0.500$, unpaired t-test; 2D), compared to CONs'. Thus, SalB delivery specifically decreases FAA running in the context of FR, but has no effect on running in general during *ad libitum* food availability.

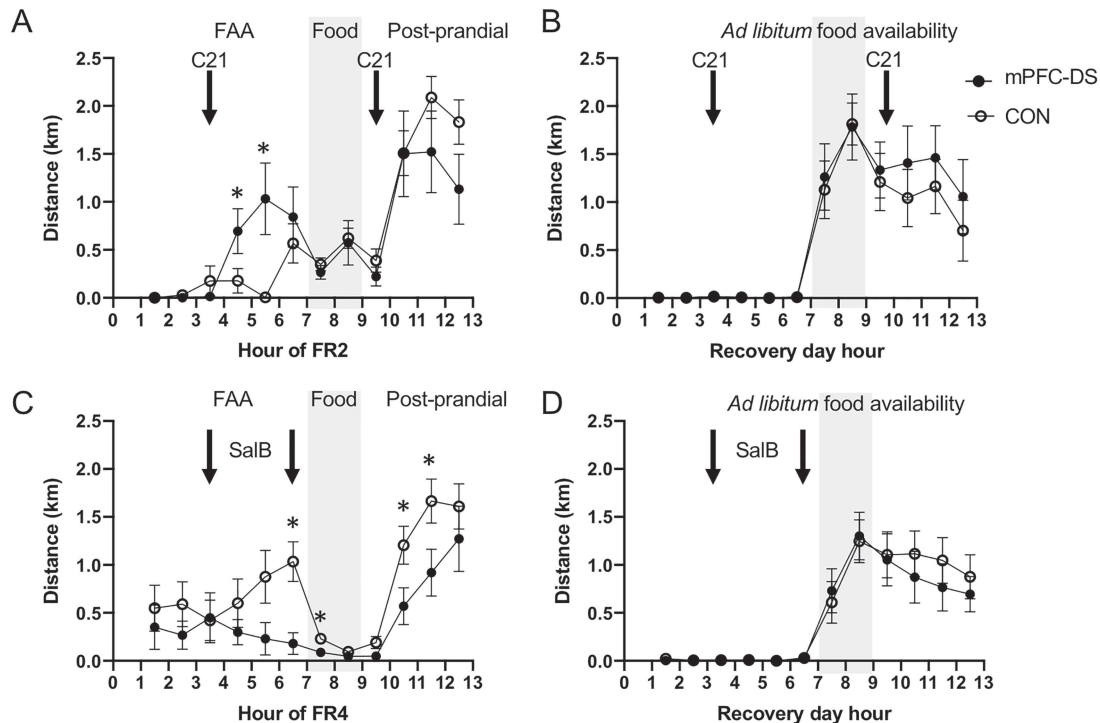


Figure 2. Bidirectional mPFC-DS control of FAA running occurs only during FR, not following recovery. C21 was administered to drive activity in mPFC-DS cells on FR2 (A) and following weight recovery (B). SalB was administered to suppress activity in mPFC-DS cells on FR4 (C) and following weight recovery (D). Injection times are indicated by black arrows. Hours of the day are indicated in the X-axis, with the 7–9 pm h of food availability highlighted in gray. Error bars indicate mean \pm SEM; asterisks indicate significant differences, compared to CON values ($P < 0.05$).

Delivery of SalB on FR4 significantly decreased running distance during the feeding time (7–9 pm) by 59.3% ($t(23) = 2.225$, $P = 0.036$, unpaired t -test), with a significant decrease during the first hour of food availability (7–8 pm time bin; ($t(23) = 2.083$, $P = 0.048$, unpaired t -test), but no effect on running duration ($t(23) = 0.983$, $P = 0.336$, unpaired t -test; Fig. 2C). Delivery of SalB in weight-restored recovered mice during the same hours had no effect on running distance ($t(17) = 0.161$, $P = 0.987$, unpaired t -test) or duration ($t(17) = 0.055$, $P = 0.956$, unpaired t -test; Fig. 2D).

Delivery of SalB on FR4 significantly decreased postprandial (9 pm–1 am) running distance by 39.8%, compared to CON ($t(23) = 2.188$, $P = 0.039$, unpaired t -test, Fig. 2C), with a significant decrease during the hours of 10–11 pm ($t(23) = 2.102$, $P = 0.047$, unpaired t -test) and 11 pm–12 am ($t(23) = 2.087$, $P = 0.048$, unpaired t -test). SalB delivery also decreased postprandial running duration by 36.3% ($t(23) = 2.348$, $P = 0.028$, unpaired t -test;). By contrast, delivery of SalB to the same animals during the same hours but after weight restoration had no effect on running distance ($t(17) = 1.460$, $P = 0.2678$, unpaired t -test) or running duration ($t(17) = 0.987$, $P = 0.337$, unpaired t -test; Fig. 2D). Thus, SalB delivery decreases running during FAA, food allowance, and postprandial periods, specifically during FR, without affecting running during recovery.

Bidirectional Modulation of the mPFC-DS Pathway Does Not Alter Body Weight or Food Consumption

To determine the impact of wheel running upon body weight, weight loss was calculated as the percent change in weight between the baseline weight measured immediately before the

start of FR1 and the FR weight measured at 7 pm, immediately following FAA. DREADD activation of mPFC-DS cells via C21 on FR2 did not measurably alter the percent weight loss from baseline ($t(23) = 0.468$; $P = 0.644$, unpaired t -test) or alter percent weight gain over the 2 h of food allowance ($t(23) = 0.150$; $P = 0.882$, unpaired t -test). Likewise, suppression of mPFC-DS cells on FR4 did not measurably alter percent weight loss from baseline ($t(23) = 0.023$; $P = 0.982$, unpaired t -test) or alter percent weight gain over the 2 h of food allowance ($t(23) = 0.549$; $P = 0.589$, unpaired t -test). Food consumption over the period of food allowance also was not different between mPFC-DS and CON groups following cell activation on FR2 ($t(10.33) = 1.357$; $P = 0.204$, Welch's t -test) or suppression on FR4 ($t(23) = 1.159$; $P = 0.258$, unpaired t -test).

C21 Activation of mPFC Pyramidal Cells via CaMKII α Promoter-Driven Gq-DREADD Increases FR-Evoked Running during FAA

We then tested whether activation of the full population of mPFC pyramidal cells would increase FAA hyperactivity, or broaden the hyperactive response to include running during *ad libitum* food availability. After delivery of C21 during FAA of FR2 to activate all mPFC pyramidal cells targeted by the CaMKII α promoter, we observed a 255% increase in running distance ($t(20) = 2.919$, $P = 0.009$, unpaired t -test) versus CON subjects, with a significant increase at the 5–6 pm time bin ($t(20) = 3.744$, $P = 0.001$, unpaired t -test). Running duration increased by 190% ($t(20) = 3.152$, $P = 0.005$, unpaired t -test), compared to CON subjects' (Fig. 3A). DREADD-driven effects observed on FR2 were

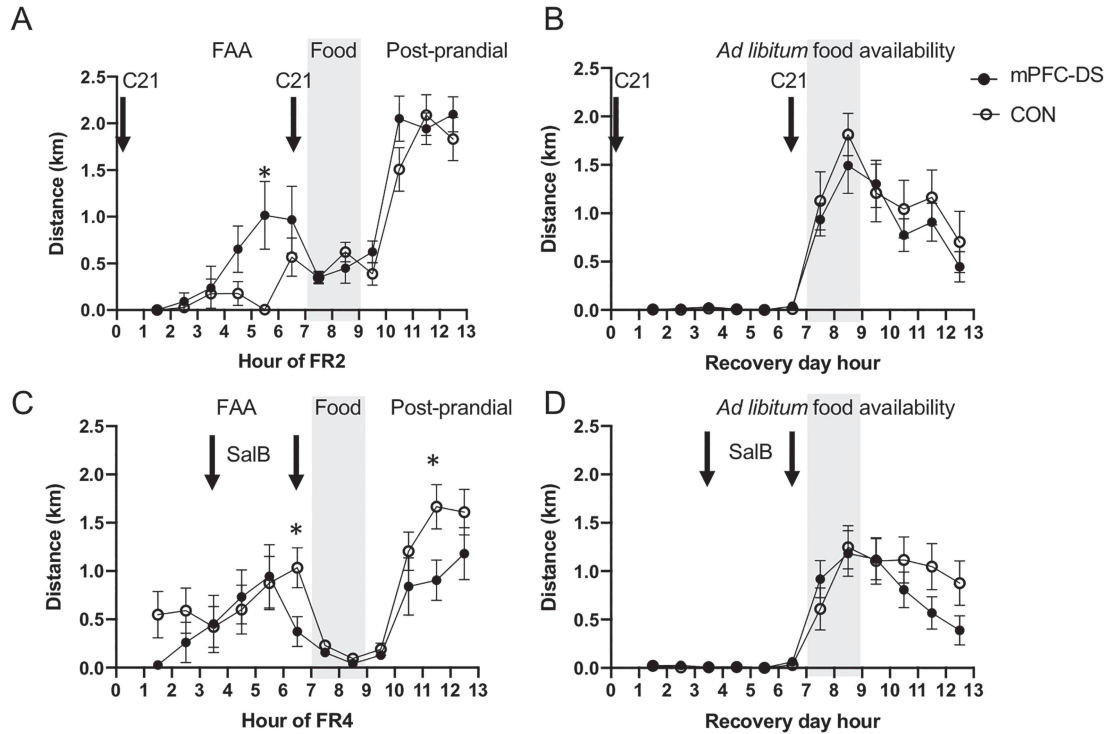


Figure 3. Activation of general mPFC pyramidal cells drives FAA running during FR, but not following recovery, while suppression has a broader temporal effect. C21 was administered to drive activity of mPFC pyramidal cells on FR2 (A) and following weight recovery (B). SalB was administered to suppress activity of mPFC pyramidal cells on FR4 (C) and following weight recovery (D). Injection times are indicated by black arrows. Hours of the day are indicated in the X-axis, with the 7–9 pm h of food availability highlighted in gray. The values are mean \pm SEM. Asterisks indicate significant differences, compared to CON values ($P < 0.05$).

no longer present on FR3, 24 h after C21 administration (for distance: $t(22) = 0.631$, $P = 0.534$, unpaired t-test; for duration: $t(22) = 0.821$, $P = 0.421$, unpaired t-test).

The C21 effect on running distance was specific to the FR state, as delivery of C21 to the same animals after weight restoration had no effect on running distance during the same 4–7 pm h of FAA ($t(20) = 0.750$, $P = 0.462$, unpaired t-test, Fig. 3B). Running duration from 4 to 7 pm in recovered CaMKII subjects treated with C21 differed from CON subjects' by 154% ($t(17.99) = 2.952$, $P = 0.009$, Welch's t-test). However, the C21 effect on running duration during recovery was relatively small compared to the effect during FR, with a difference in means of only 6.587 ± 2.231 active minutes during recovery, versus 44.27 ± 14.05 active minutes during FR.

For the CaMKII group, delivery of C21 during FR2 food allowance (7–9 pm) had no effect on running distance ($t(20) = 0.837$, $P = 0.412$, unpaired t-test) or duration ($t(20) = 1.332$, $P = 0.198$, unpaired t-test), compared to CON subjects (Fig. 3A). Likewise, delivery of C21 in weight-restored recovered mice during the same hours had no effect on running distance ($t(20) = 0.871$, $P = 0.394$, unpaired t-test) or duration ($t(20) = 0.896$, $P = 0.381$, unpaired t-test; Fig. 3B). Thus, activation of mPFC pyramidal cells via C21 delivery specifically increases FAA running without affecting subsequent running during the period of food allowance.

Delivery of C21 on FR2 had no effect on postprandial (9 pm–1 am) running distance ($t(20) = 0.994$, $P = 0.332$, unpaired t-test), or duration, although there was a trend toward increase for the latter ($t(20) = 1.994$, $P = 0.060$, unpaired t-test; Fig. 3A). Likewise,

delivery of C21 to the same animals after weight restoration had no effect on 9 pm–1 am running distance ($t(20) = 0.592$, $P = 0.560$, unpaired t-test) or running duration ($t(20) = 0.330$, $P = 0.745$, unpaired t-test; Fig. 3B). Thus, activation of CaMKII pyramidal cells specifically increases FAA running without affecting subsequent running during the 2 h of food availability or the postprandial period. Together, this indicates that the robust C21 effect observed for activation of mPFC-DS-projecting cells was matched, but not enhanced, when the suppression included mPFC pyramidal cells that project elsewhere.

SalB Suppression of mPFC Pyramidal Cells via CaMKII α Promoter-Driven KORD-DREADD Decreases FR-Evoked Running

For the CaMKII group, delivery of SalB on FR4 had no effect on pooled FAA (4–7 pm) running distance ($t(24) = 0.452$, $P = 0.655$, unpaired t-test) or duration ($t(24) = 0.367$, $P = 0.717$, unpaired t-test), compared to CON subjects' (Fig. 3C). However, there was a significant 40% decrease in running distance specifically at the 6–7 pm time bin, when hunger is most intense ($t(24) = 2.272$, $P = 0.032$, unpaired t-test). Delivery of SalB to mice after weight restoration had no effect on running distance ($t(10.12) = 1.201$, $P = 0.257$, Welch's t-test) or duration ($t(17) = 0.1049$, $P = 0.309$, unpaired t-test; Fig. 3D).

For the CaMKII group, delivery of SalB during food allowance of FR4 (7–9 pm) had no effect on running distance ($t(24) = 1.645$, $P = 0.113$, unpaired t-test) or duration ($t(24) = 0.907$, $P = 0.374$, unpaired t-test), when compared to CON subjects' (Fig. 3C).

Likewise, delivery of SalB in recovered mice during the same hours produced no effect on running distance ($t(24) = 0.108$, $P = 0.915$, unpaired t-test) or duration ($t(24) = 0.597$, $P = 0.644$, unpaired t-test; Fig. 3D).

Following delivery of SalB on FR4, CaMKII mice trended toward a reduction of postprandial (9 pm–1 am) running distance ($t(24) = 1.796$, $P = 0.085$, unpaired t-test), with a significant decrease occurring for the hour of 11 pm–12 am ($t(24) = 2.267$, $P = 0.033$, unpaired t-test). There was no significant reduction in postprandial running duration ($t(24) = 1.427$, $P = 0.167$, unpaired t-test; Fig. 3C). Likewise, delivery of SalB during the same time bin but after weight restoration had no significant effect, but a strong trend toward reduction for postprandial running distance ($t(24) = 1.943$, $P = 0.064$, unpaired t-test) and running duration ($t(24) = 1.905$, $P = 0.069$, unpaired t-test; Fig. 3D). Thus, suppression of mPFC pyramidal cells via SalB delivery produces a measurable reduction in wheel running only during the last hour of FAA, when hunger is most intense, and during the 11–12 h postprandial time bin. This indicates that the SalB effect upon mPFC pyramidal cells of reducing FAA was present, but much muted, when the suppression included mPFC pyramidal cells that project elsewhere.

Bidirectional Modulations of mPFC Pyramidal Cells via CaMKII α Promoter-Driven Gq-DREADD and KORD-DREADD Do Not Alter Body Weight or Food Consumption

Up to the time of entry into ABA2, CON and chemogenetically modulated groups of mice exhibited no group difference in body weight or food consumption. Specifically, there was no significant differences in weight on ~P36 when mice were introduced to wheels, between mPFC-DS versus CON mice ($t(22) = 1.04$, $P = 0.310$, unpaired t-test) or CaMKII versus CON mice ($t(25) = 0.155$, $P = 0.878$, unpaired t-test). Likewise, there was no significant group differences in weight (mPFC-DS vs. CON: $t(22) = 1.316$, $P = 0.201$, unpaired t-test; CaMKII vs. CON: $t(27) = 0.780$, $P = 0.442$, unpaired t-test) or running distance (mPFC-DS vs. CON: $t(17) = 0.069$, $P = 0.946$, unpaired t-test; CaMKII vs. CON: $t(24) = 1.057$, $P = 0.301$, unpaired t-test) at termination of ABA1, indicating no major differences in vulnerability to consider between groups as they entered ABA2 for chemogenetic manipulations.

Despite the robust effect that DREADD activation of mPFC pyramidal cells via C21 during ABA2 had on FAA, this change in behavior did not measurably alter percent weight loss for FR2 ($t(7.54) = 0.206$; $P = 0.846$, Welch's t-test) or alter percent weight gain over the 2 h of food allowance ($t(22) = 0.404$; $P = 0.690$, unpaired t-test), relative to CON subjects. Likewise, suppression of mPFC pyramidal cells by SalB on FR4 did not measurably alter percent weight loss on FR4 ($t(24) = 1.639$; $P = 0.114$, unpaired t-test), or percent weight gain over the 2 h of food allowance on FR4 ($t(24) = 0.147$; $P = 0.885$, unpaired t-test), compared to CON. Food consumption during the 2 h window also was not different between CaMKII and CON groups following cell activation on FR2 ($t(9.016) = 0.636$; $P = 0.540$, Welch's t-test) or suppression on FR4 ($t(24) = 1.367$; $P = 0.184$, unpaired t-test).

Elevated Plus Maze

Elevated plus maze was administered to all subjects to assess general anxiety level before either DREADD ligand was administered, during the hours of 6–9 am of FR1. As compared to

CON subjects, there were no significant differences in percent duration of time spent in the open arms of the EPM for either the CaMKII ($t(29) = 0.688$; $P = 0.497$, unpaired t-test) or mPFC-DS groups ($t(10.42) = 1.118$; $P = 0.289$, Welch's t-test), thus confirming that the effect observed following DREADD ligand administration had no contribution from pre-existing differences in the general anxiety level.

Viral Expression

Virally mediated expression of cre-dependent DREADDs was observable in layers 2–6 of mPFC (Fig. 4A–B). The mCherry reporter identifies expression of the Gq receptor, and the mCitrine reporter identifies expression of the KORD receptor. Of all 18 hemispheres of the mPFC-DS group, 94% expressed both viruses in the Cg1, 100% expressed both viruses in the PL, and 94% expressed both viruses in the IL. Cre-dependence of the viral expression was confirmed, as cre-dependent DREADD virus was unable to replicate in the absence of the retrogradely transported (rg)-cre-virus ($N = 5$; Fig. 4C). We confirmed mCitrine positive (KORD receptor-expressing) axon terminals in the gray matter of the medial DS (Fig. 4H). Several of the cells supported viral expression of both mCherry and mCitrine, indicating that a single cell can support replication of both cre-dependent DREADD viruses as well as the rg-cre virus without visible damage to cells (Fig. 4B). The absence of DREADDs in GABA-INS was confirmed by the absence of GAD/DREADD colabeling (Fig. 4C).

Virally mediated expression of CaMKII α promoter-driven DREADDs was observable in layers 2–6 of mPFC (Fig. 4D–E). Viral expression spanned the dorsal-ventral axis of the mPFC, centering around the prelimbic cortex (PL) subregion, with anteroposterior axis center of 2.34+ Bregma. Of all 30 hemispheres targeted in the CaMKII group, 100% expressed both viruses in the cingulate cortex (Cg1) and PL regions, and 96% expressed both viruses in the infralimbic cortex (IL). Virally mediated expression of CaMKII α promoter-driven DREADDs was found specifically in pyramidal cells, identifiable by their distinct cell body shape and singular apical dendrites. Several of the cells supported viral expression of both mCherry and mCitrine, indicating that a single cell could support replication of both viruses without visible detriment to cell health (Fig. 4E).

Expression of c-Fos after DREADD Ligand Delivery

Immunocytochemistry was conducted to assess the extent to which subcutaneous drug delivery 2 h prior to euthanasia could alter c-Fos activity in DREADD-expressing cells, as well as GABA-INS (Fig. 4C,F). Basal c-Fos activity in mPFC pyramidal cells was assessed in the GFP-CON mice (expressing GFP but not DREADD in mPFC pyramidal cells; $N = 5$), which received C21 2 h before euthanasia. For these subjects, $7.7\% \pm 1.6\%$ of GFP+ pyramidal cells expressed c-Fos.

For the CaMKII subjects that received SalB prior to perfusion (CaMKII-SalB; $N = 7$), c-Fos immunoreactivity was evident within $3.9\% \pm 2.6\%$ of pyramidal neurons, identified by GFP immunoreactivity to the KORD-reporter protein, mCitrine. This level of c-Fos immunoreactivity did not differ significantly from basal mPFC c-Fos expression ($t(10) = 1.153$, $P = 0.276$, unpaired t-test), although we did detect a floor effect, as four out of the seven CaMKII-SalB cases had zero c-Fos expression among KORD/mCitrine/GFP expressing cells, while none of the five GFP-CON animals exhibited zero values. Of the nine mPFC-DS group mice,

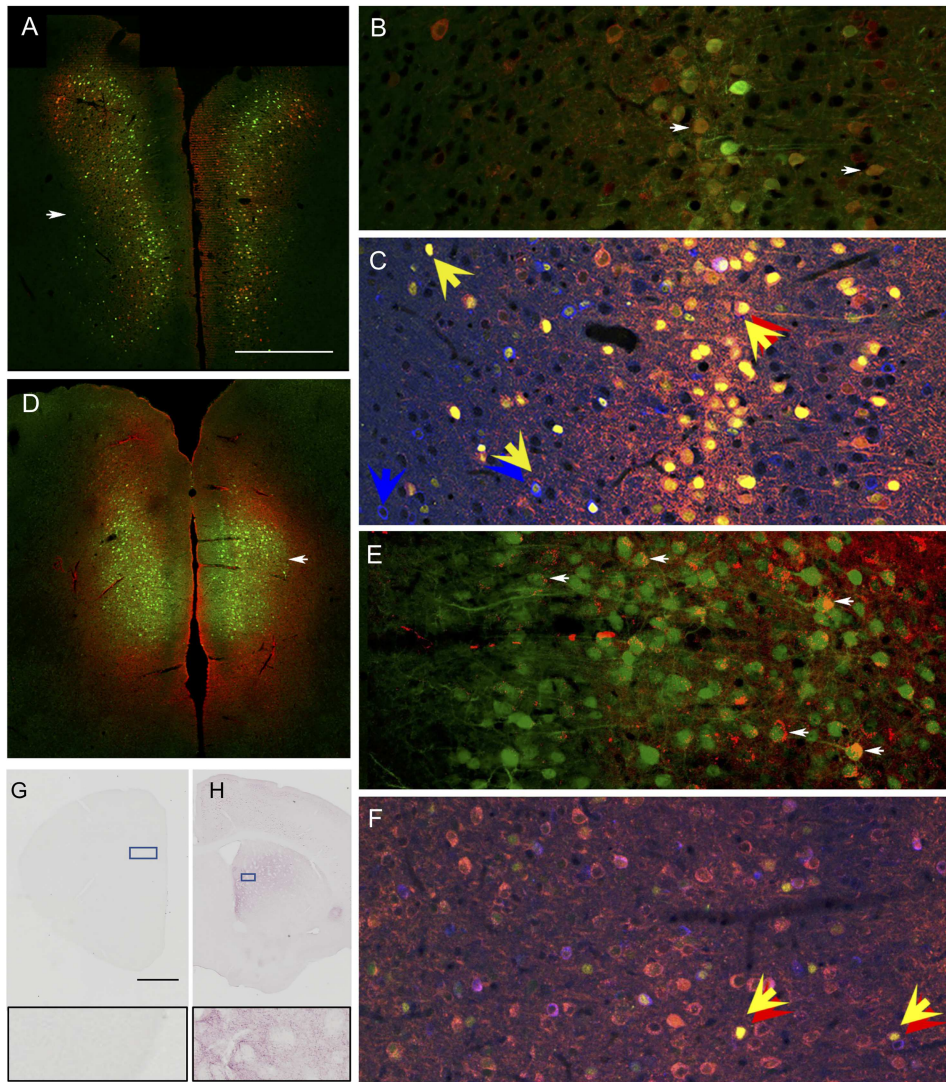


Figure 4. Immunofluorescence reveals pyramidal cell-specific DREADD expression and verifies DREADD-driven modulation of pyramidal cell activity. mCherry and mCitrine protein immunoreactivity in the mPFC reflect the virally mediated transfer of genes encoding DREADDs that were either excitatory (Gq-mCherry) or inhibitory (KORD-mCitrine). Viral expression was either Cre-dependent with retrograde Cre delivered into the DS, for expression specifically in pyramidal neurons projecting to DS (mPFC-DS; panels A and B) or CaMKII-promoter driven (panels D and E) for pyramidal neuron specific expression. Panels B and E show details of the prelimbic (PL) subregion of mPFC (arrows in panels A and D). mCherry-immunoreactivity (red) appears as puncta in the perikaryal cytoplasm. In contrast, mCitrine-immunoreactivity (green) appears to fill the nucleus, perikaryal cytoplasm and apical dendrites of pyramidal neurons. Arrows in B and E point to some of the dually immunolabeled cell bodies. C and F. Triple immunofluorescence was performed to simultaneously detect c-Fos protein in nuclei (yellow, examples highlighted by yellow arrows) and mCherry (red, red arrows), together with glutamic acid decarboxylase (GAD), the rate-limiting synthetic enzyme of GABAergic interneurons (GABA-INS, blue, blue arrows) in the PL by confocal microscopy. C21 was delivered to activate DREADD-Gq receptors 2–3 h prior to euthanasia. mCitrine, the KORD virus reporter (green), was also detected, but not amplified by IF. Panel C depicts PL of mPFC-DS tissue. Panel F depicts PL of tissue transfected with the CaMKII α -Gq-DREADD-mCherry transgene. Overall, c-Fos immunoreactivity is more prevalent following activation of the mPFC-DS subpopulation, relative to activation of the general population of pyramidal neurons with CaMKII α -Gq-DREADD-mCherry. GABA-INS with c-Fos in nucleus are also apparent (yellow-blue double arrow), suggesting recruitment of GABA-INS. G. Absence of KORD viral replication in mCitrine-expressing cells in mPFC of “No-cre-CON” after immunohistochemical detection of mCitrine, the reporter for KORD, using an anti-GFP antibody. The rectangle at the bottom of panel G shows mPFC at a higher magnification. H. mCitrine-expressing axons in DS, revealed by immunohistochemical detection of mCitrine, using anti-GFP, and visualized by the HRP reaction product VIP from a section of a brain transfected with KORD-mCitrine. Anti-GFP also detected the eGFP reporter for the retrograde cre virus, localized to nuclei of transfected pyramidal neurons. The insets of G and H correspond to the boxes in the panels. Calibration bar equals 100 μ m in panels B, C, E, and F and 600 μ m in panels A and D. Calibration bar in panel G applies to both panels G and H, equaling 100 μ m.

only two received SalB prior to perfusion, with c-Fos immunoreactivity evident within $2.8\% \pm 1.0\%$ of mCitrine/GFP+ cells.

Despite the lack of C21-driven running in weight-recovered mice with *ad libitum* food access, we did observe a C21-driven increase in pyramidal cell c-Fos expression in weight-recovered

mice for both experimental groups. Of the CaMKII subjects that received C21 prior to perfusion (CaMKII-C21; $N = 8$), c-Fos expression in pyramidal cells was 2.55 times greater versus GFP-CON, with $19.7\% \pm 4.1\%$ of mCherry positive cells expressing c-Fos ($t(8.898) = 2.731$, $P = 0.023$, Welch's t-test, Fig 5A). This ratio is

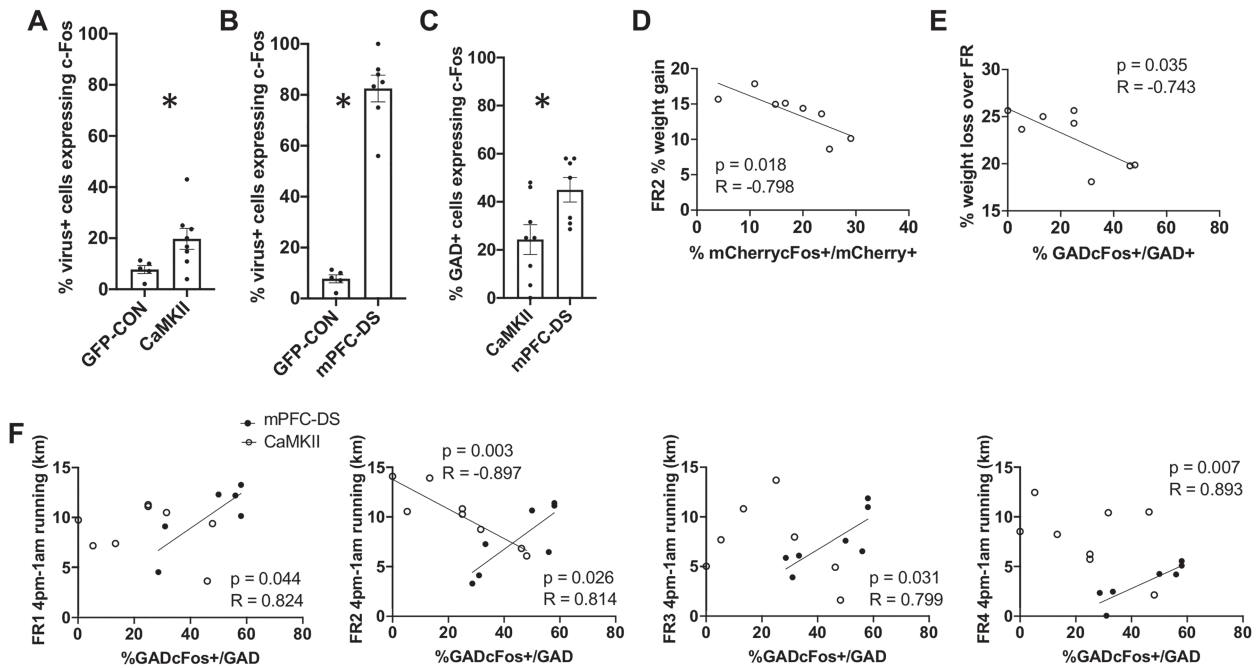


Figure 5. Quantification of c-Fos, GAD and mCherry reveals microcircuitry activated by C21 and correlation of microcircuitry activity with behavior. A. C21-driven c-Fos expression is greater in the pyramidal cells of the CaMKII α -Gq-DREADD group versus the CaMKII α -GFP control group (GFP-CON). B. C21 driven c-Fos expression is greater in the pyramidal cells of the mPFC-DS group versus the CaMKII α -GFP control group. C. C21-driven recruitment of GABA-INs is greater for the mPFC-DS group versus the CaMKII group. Asterisks in panels A, B and C denote $P < 0.05$. Values of the graphs are mean \pm SEM. D. In the CaMKII group, percent of mChery+ pyramidal cells expressing c-Fos correlates negatively with percent weight gain on FR2, but not other days. E. In the CaMKII group, percent of GAD+ GABA-INs expressing c-Fos correlates negatively with weight loss over the 4-day course of FR. F. In the CaMKII group (open circle), percent of GABA-INs expressing c-Fos correlates significantly and negatively with running that spans 4 pm–1 am (includes FAA, food availability, and postprandial time bins) during C21 activation on FR2. In the mPFC-DS group (filled circle), the percent of the GABA-INs expressing c-Fos correlates significantly and positively with running that spans 4 pm–1 am on all 4 days of FR. Each graph shows the outcome of the correlation analysis for each of the 4 days of FR. Solid line indicates significant correlation, no line indicates $P > 0.1$.

consistent with previously reported data using CaMKII-DREADD to activate pyramidal cells in the mPFC (Pati et al. 2018). By contrast, pyramidal c-Fos expression was 10.67 times greater in the C21-activated mPFC-DS group ($N = 7$), with $82.5\% \pm 5.2\%$ of mChery positive cells expressing c-Fos ($t(7.055) = 13.63$, $P < 0.001$, Welch's t-test, Fig 5B).

For explanation of the difference in c-Fos immunoreactivity of the mPFC-DS group versus the CaMKII group, we turned to mPFC microcircuitry, and asked whether C21 delivery evoked a different response when acting on the mPFC-DS subpopulation, versus general pyramidal cell activation. Interestingly, the percent of GAD-immunoreactive cells co-expressing c-Fos was greater following C21 delivery to the mPFC-DS group (45.0%), versus the CaMKII group (24.3%; $t(13) = 2.529$, $P = 0.025$, unpaired t-test; Fig 5C), indicating that, compared to the general pyramidal cell population, activity from the mPFC-DS subpopulation evokes a greater GABA-IN response.

Individual Differences in Neuronal Activity as Revealed by c-Fos Expression Relate to Individual Differences in Wheel Running

While C21 evoked robust 245% and 255% increase in FR2 FAA running via activation of the mPFC-DS and the general population of mPFC pyramidal cells, respectively (Figs 2 and 3), the same measurements also revealed multi-fold differences in individuals' extent of C21-evoked running. To better understand the nature of these individual differences, we assessed whether

these differences related to the extent of C21/DREADD-driven c-Fos activity of neurons in the mPFC (see Table 1 for P and R values). Contrary to our expectation, c-Fos expression in mChery+ pyramidal cells of either mPFC-DS or CaMKII groups did not correlate significantly with running distance during FAA or the 4 pm-1 am period. This indicates that another group of cells might contribute more strongly toward individual differences in running.

For the CaMKII group, the percent of GAD+ cells expressing c-Fos correlated negatively with running distance during the 4 pm–1 am h of C21 activation on FR2, (Fig 5F; Table 1), with no correlation between GAD+/cFos+ cells and running during this period of other FR days. Within this window of C21 activation on FR2, GAD+ c-Fos immunoreactivity correlated specifically with running during the 4–7 pm FAA period ($P = 0.003$; $R = -0.893$), and not with running during the 2 h of food availability ($P = 0.955$; $R = -0.024$) or the postprandial period ($P = 0.131$; $R = 0.581$). This negative correlation, only on FR2, indicates that the C21-induced recruitment of GABA-INs by the general population of pyramidal cells contributed toward individual differences in the dampening of hyperactivity, particularly during the FAA hours.

By contrast, for the mPFC-DS group, the percent of GAD+ cells expressing c-Fos correlated positively with running. Moreover, in contrast to the CaMKII group, GAD+/c-Fos+ cells correlated with running during 4 pm-1 am not only on FR2, but on all FR days (Fig 5F; Table 1). This effect was specific to running in the context of FR, as there was no correlation between running and GAD+ cell c-Fos expression during the days with *ad libitum*

Table 1 Correlations between c-Fos expression and running/weight change

Variable	Variable		PFC-DS group		CaMKII group	
			P value	R value	P value	R value
Percent of mCherry+ pyramidal cells expressing c-Fos	Running (km; 4 pm–1 am)	FR 1	0.665	−0.228	0.967	−0.180
		FR 2	0.374	−0.400	0.096	−0.627
		FR 3	0.099	−0.671	0.673	−0.178
		FR 4	0.325	−0.439	0.582	−0.231
	% Weight loss	FR 1	0.068	0.720	0.861	−0.074
		FR 2	0.774	−0.134	0.449	0.314
		FR 3	0.579	−0.256	0.096	−0.628
		FR 4	0.587	−0.251	0.186	−0.521
	% Weight gain over 2 h of food availability	FR 1	0.366	0.406	0.383	0.359
		FR 2	0.766	−0.139	0.018	−0.798
		FR 3	0.539	−0.283	0.741	0.140
		FR 4	0.225	0.277	0.464	0.304
% GABA-IN expressing c-Fos	Running (km; 4 pm–1 am)	FR 1	0.044	0.824	0.654	−0.189
		FR 2	0.026	0.814	0.002	−0.897
		FR 3	0.031	0.799	0.497	−0.283
		FR 4	0.007	0.893	0.297	−0.422
	% Weight loss	FR 1	0.641	−0.217	0.558	−0.246
		FR 2	0.874	0.075	0.507	0.278
		FR 3	0.752	0.148	0.004	−0.883
		FR 4	0.844	−0.092	0.035	−0.743
	% Weight gain over 2 h of food availability	FR 1	0.359	−0.412	0.465	−0.304
		FR 2	0.654	−0.208	0.477	−0.296
		FR 3	0.086	0.691	0.365	0.371
		FR 4	0.886	0.067	0.238	0.471

Note: List of variables and the observed results of correlations for both the mPFC-DS subpopulation and general mPFC pyramidal cell population. Percent weight loss is calculated as the weight at 7 pm on the FR day subtracted from the weight at the start of ABA2, all divided by the weight at the start of ABA2. Percent weight gain is calculated as the weight at 9 pm subtracted from the weight at 7 pm of the same day, all divided by the weight at 7 pm. Significant values are bolded.

food access preceding FR (preceding FR by 1 day: $P = 0.387$, $R = 0.436$; preceding by 2 days: $P = 0.713$, $R = -0.172$) or on days after weight-restoration (with C21 delivery: $P = 0.163$, $R = 0.591$; with SalB delivery: $P = 0.458$, $R = 0.339$; with no drug: $P = 0.114$, $R = 0.650$). Because C21-activation of pyramidal neurons in the mPFC augments FR-evoked running, the positive correlation between running and GAD+/c-Fos+ cells, which dampen pyramidal neurons, was contrary to expectation (reconciled in Fig. 10 and Discussion).

Individual Differences in Neuronal Activity as Revealed by c-Fos Expression Relate to Individual Differences in Weight Loss over FR and Weight Gain during the Hours of Food Access

For the CaMKII group, individual differences in percent weight loss correlated negatively with percent of GAD+ cells expressing c-Fos on FR3 and FR4 (Fig 5D; Table 1), indicating that GABAergic inhibition, recruited by C21 activation of pyramidal cells, may have been protective against weight loss during the days with severest weight loss. By contrast, for the mPFC-DS group, individual differences in percent weight loss did not correlate with percent of GAD+ cells expressing c-Fos on either day.

As stated earlier, analysis of weight gain revealed no group differences across the C21-treated versus CON for the CaMKII group or the mPFC-DS group. Yet, for the CaMKII group, the percent of mCherry+ pyramidal cells expressing c-Fos correlated negatively with the percent weight gain over the 2 h period of food availability on FR2, when C21 was active, but not on

other FR days (Fig 5E; Table 1), indicating that pyramidal cell activation by C21 on FR2 may have hampered food consumption. By contrast, the percent of DS-projecting mCherry+ pyramidal neurons expressing c-Fos showed no correlation. This could reflect greater C21 activation of non-DS-projecting mPFC pyramidal cells with targets to a feeding center, such as the lateral hypothalamus, which regulates food consumption when activated (Cassidy and Tong 2017) and receives strong projection from mPFC (Gabbott et al. 2005).

Electron Microscopic Verification of Gq-DREADD Expression

For neurons to be responsive to DREADD ligands, DREADDs need to be expressed at the plasma membrane. Electron microscopy verified that immunoreactivity for mCherry, the reporter for cre-dependent Gq-DREADD expression, was localized to the plasma membrane of cell bodies containing nuclei with smooth contour, characteristic of pyramidal neurons (Fig 6A; White 1989). Cre-dependent DREADD expression was also evident along the plasma membrane of dendritic spines, also indicating expression in excitatory pyramidal cells (Fig 6B). Synapses formed by axon terminals with mCherry immunoreactivity exhibited thick postsynaptic densities (PSDs; Fig 6C), indicated that these synapses are excitatory, as would be expected for glutamatergic synapses formed by pyramidal neurons (White 1989). mCherry-immunoreactive pyramidal neurons targeted dendritic spines, indicating pyramidal-to-pyramidal synaptic targets (Fig 6D). mCherry-immunoreactive pyramidal

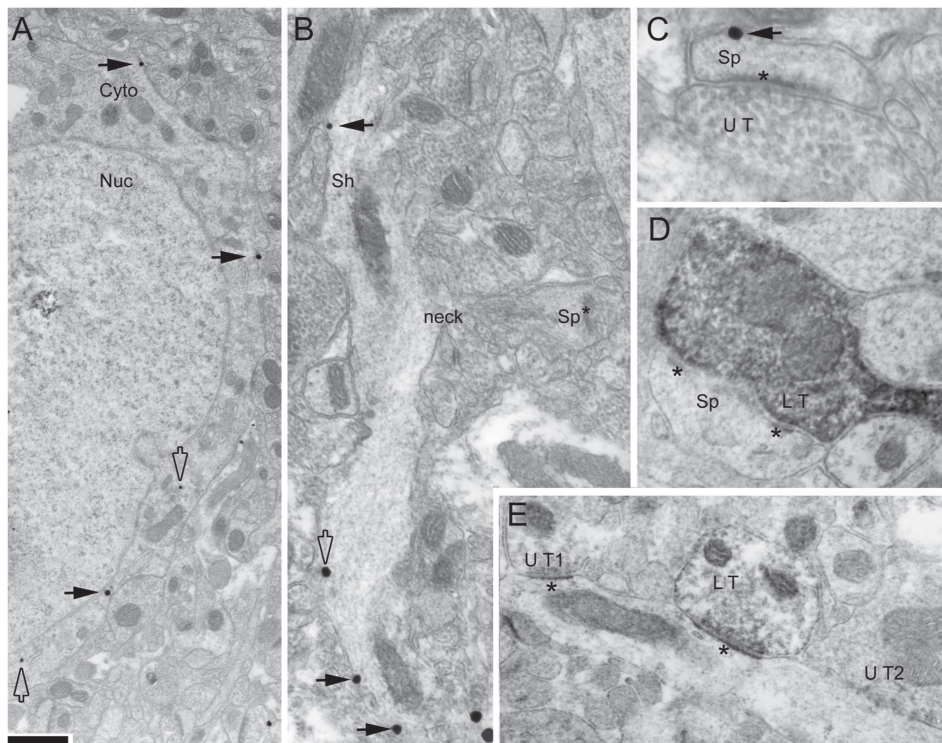


Figure 6. Electron microscopic verification of the localization of DREADD-mCherry to the plasma membrane. Silver-intensified gold labels (SIG; panels A through C) and HRP-DAB reaction products (panels D and E) were used to immunolabel mCherry, the reporter of the Gq-DREADD. The non-diffusible SIG reveals the location of mCherry along intracellular surfaces of the plasma membrane (black arrows in panel A and other panels) of a neuronal cell body, likely to be of a pyramidal neuron, based on the smooth contour of the nuclear (Nuc) envelope. The open arrows point to SIGs located in the cytoplasm (Cyto), removed from the plasma membrane. Plasmalemmal labeling for mCherry is evident in dendritic shafts (Sh, panel B) from which a spine head forming an asymmetric synapse with thick PSD protrudes via its spine neck, indicating that this dendrite is of a spiny neuron, presumably pyramidal. Spine heads (Sp, panel C) forming asymmetric synapses with unlabeled terminals (UT) are immunoreactive for mCherry along the plasma membrane. mCherry also occurs presynaptically, in axon terminals forming asymmetric, putatively excitatory synapses with prominent PSDs onto dendritic spines (LT = labeled terminal, panel D), indicative of a pyramidal-to-pyramidal synapse. Other mCherry axon terminals form asymmetric synapses onto dendritic shafts (panel E), indicative of pyramidal-to-GABAergic interneuron synapse. Calibration bar = 1 μ m for panel A, 480 nm in B, 240 nm in C, 300 nm in D, and 400 nm in E.

neurons also targeted dendritic shafts that were mCherry-immunonegative (Fig. 6E). As GABA-INs are known to receive excitatory synaptic inputs directly onto their dendritic shafts and cell bodies (White 1989), this relationship was indicative of pyramidal-to-GABA-IN synaptic targets, thus providing the cellular substrate for c-Fos expression in GAD+ cells (Fig. 5C).

Greater GABAergic Innervation of Non-DS-Projecting Layer 5 mPFC Pyramidal Cells

Electron microscopy was then used in the mPFC-DS group ($N=7$), to assess GABAergic axo-somatic contacts to layer 5 mPFC pyramidal cells, either expressing mCherry, confirming projection to DS (Fig. 7), or lacking mCherry expression (Fig. 8). GABA-INs were identified by DAB precipitate, reflecting GAD immunoreactivity, whereas mCherry immunoreactivity was identified by another electron-dense immunolabel, SIG (silver-intensified colloidal gold). GABAergic innervation was quantified as percent of the somatic plasma membrane contacted directly by GAD+ terminals. Surprisingly, we found that the mCherry positive, DS-projecting subpopulation of mPFC pyramidal cells had 42.3% less axo-somatic GABAergic innervation than neighboring unlabeled pyramidal cells ($t(12)=2.914$; $P=0.013$; unpaired t-test, Fig. 9A). This was due to a 43.8% lower density of

GABAergic innervation (number of GABAergic contacts per mm of plasma membrane profile; $t(12)=3.392$; $P=0.005$; unpaired t-test, Fig. 9B), while size of synaptic terminal was not different between groups ($t(12)=0.243$; $P=0.812$; unpaired t-test, Fig. 9C). Together with the c-Fos data on GABA-INs, this indicates that, although driving mPFC-DS pyramidal cells elicits a strong response from GABA-INs in the mPFC, GABAergic action has stronger axo-somatic target to neighboring non-DS-projecting mPFC pyramidal cells, versus self-inhibition (see Fig. 10 for summary).

Electron Microscopic Quantification of GABAergic Innervation Correlates with Individual Differences in Weight

We also found that axo-somatic GABAergic innervation of both mCherry+ and mCherry- cells correlates negatively with percent weight loss (Fig. 9D), suggesting that GABAergic innervation is protective against the precipitous weight loss that can become fatal in the ABA model. On FR1, mice had the least exposure to FR, and had only lost between 2% and 7% of weight. This measure did not correlate with GABAergic innervation of DS-projecting mCherry+ cells ($P=0.640$; $R=0.217$), non-DS-projecting mCherry- cells ($P=0.607$; $R=0.238$), or the

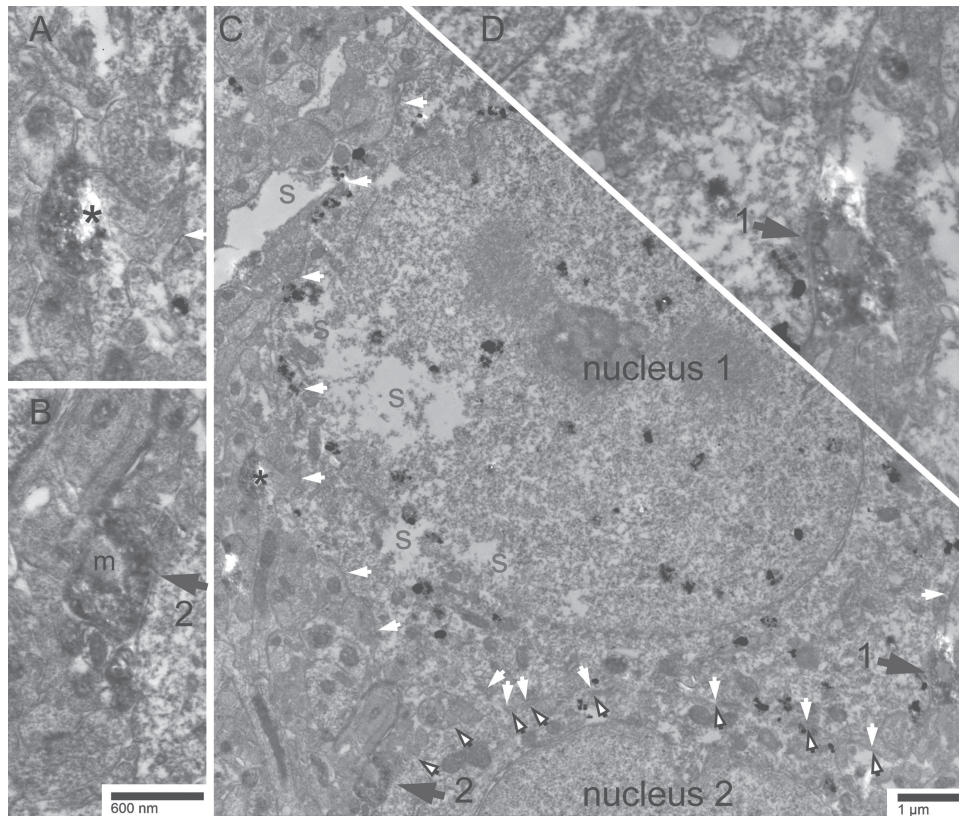


Figure 7. Sparse GABAergic innervation in a pyramidal neuron with mCherry-immunoreactivity from a brain expressing DREADD-Gq among mPFC-DS cells. SIG particles are identifiable by their maximal electron density, approximately 100 nm in size. SIGs are numerous in nucleus 1 and its surrounding cytoplasm, indicating robust mCherry expression (panel C). The plasma membrane of this cell is depicted by white arrows. Another cell body is immediately adjacent to it, indicated by the black-bordered arrows and “nucleus 2” (panel C). SIG particles are evident in the second cell’s cytoplasm as well. GAD immunoreactivity is evident based on the heavier electron-dense precipitate in the cytoplasm that is excluded from vesicle lumens and mitochondria (“m” in the axon terminal forming synapse #2). The two GABAergic innervations evident within this plane of section are indicated by the large grey arrows and shown in higher magnification in panels B and D. Arrow #1 and #2 point to a GABAergic innervations of cell 1 and cell 2, respectively. The asterisk (panel A and C) points to a GABAergic axon that is within 600 nm from the plasma membrane of Cell #1 but is interposed by an axo-spinous synapse. For each cell, the percent GABAergic innervation was measured as the percent of the somatic plasma membrane receiving GAD+ terminal contacts. Measurements for 10 cells were then averaged for each individual ($N = 7$).

average sample of both cell types ($P = 0.542$; $R = 0.281$). On FR2, when mice received C21 to drive cell firing in mPFC-DS cells, only the GABAergic innervation upon DS-projecting mCherry+ cells correlated negatively with percent weight loss ($P = 0.025$; $R = -0.815$). GABAergic innervation of the mCherry- population did not correlate with weight loss ($P = 0.709$; $R = -0.174$). As expected, the average GABAergic innervation of the two cell groups, combined, did not correlate with percent weight loss on FR2, either ($P = 0.191$; $R = -0.560$). This suggests that those individuals with strongest GABAergic inhibition of DREADD-driven mPFC-DS cells were the most protected from weight loss following C21 administration on FR2 and that the GABAergic synapses onto non-DS-projecting mPFC cells were relatively less effective in weight preservation. By FR3, percent weight loss trended toward a negative correlation with GABAergic innervation of mCherry+ cells ($P = 0.060$; $R = -0.736$), and significantly correlated with GABAergic innervation of mCherry-cells ($P = 0.034$; $R = -0.790$), with a significant correlation when GABAergic innervation of the two cell types were combined in the analysis ($P = 0.002$; $R = -0.939$). By FR4, which is the day that SalB was delivered, percent weight loss trended toward a correlation with GABAergic innervation of mCherry+ cells ($P = 0.069$; $R = -0.719$), and significantly correlated with

GABAergic innervation of mCherry- cells, only ($P = 0.030$; $R = -0.802$), or with both cell types combined ($P = 0.002$; $R = -0.938$). Major findings are summarized in Table 2.

Discussion

We demonstrate here for the first time that activation of mPFC pyramidal cells drives an increase in running distance and duration specifically during FAA of FR days, and not during the 2 h of food availability, nor postprandial time bins, and not on days with *ad libitum* food availability in weight-restored mice. This effect was fully recapitulated by driving activity of the mPFC-DS subpopulation of pyramidal cells. Conversely, suppression of mPFC pyramidal cells generally, or targeting mPFC-DS pyramidal cells, reduces wheel running specifically during FR and not on days with *ad libitum* food access. These findings reveal that mPFC activity in general, and the mPFC-DS circuit in particular, do not simply control the drive to run, but rather, control hyperactivity induced specifically by the condition of FR.

Although the phenomenon of FAA has been previously linked to activity in the DS (Gallardo et al. 2014), this is the first study to causally implicate the mPFC in FAA. Of all mPFC pyramidal cells, approximately 15% project to DS (Gabbott et al. 2005),

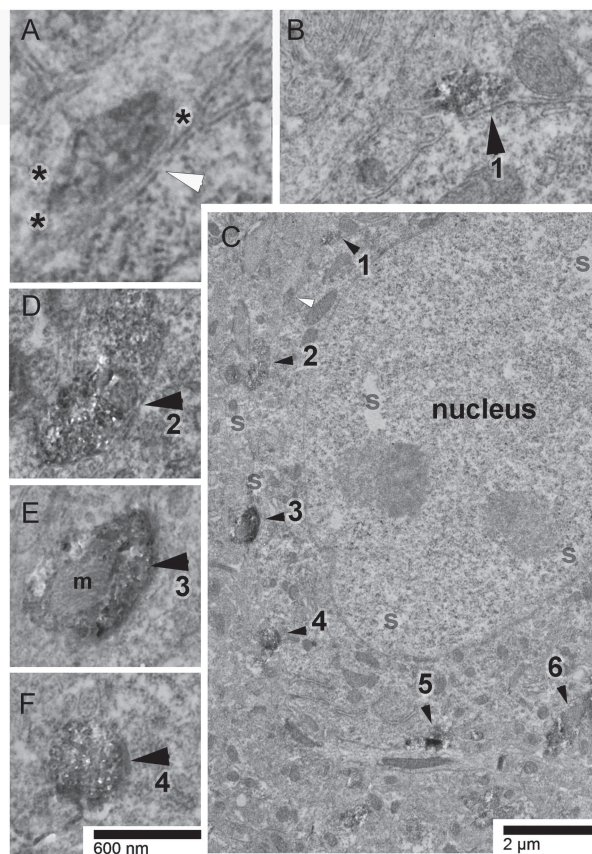


Figure 8. Prevalent GABAergic innervation of a sample pyramidal neuron lacking mCherry-immunoreactivity, from a brain expressing DREADD-Gq among mPFC-DS cells. Numerous GABAergic axon terminals form axo-somatic synapses with this cell body. The image of the cell body was captured near the surface of the vibratome tissue (indicated by the label “S” where no tissue can be seen, panel C) to minimize failure to detect SIG particles reflecting mCherry-immunoreactivity. The lack of SIG particles in this neuron indicates that this neuron is mCherry-negative. The smooth nuclear envelope and absence of GAD immunoreactivity in the cytoplasm indicates that this is a pyramidal neuron. Six additional GABAergic axo-somatic synapses along the cell body plasma membrane at this plane of section are shown, with details captured at a higher magnification of $\times 30,000$ in the surrounding small panels B, D, E, and F. GAD immunoreactivity is evident based on the heavier electron-dense precipitate in the cytoplasm that is excluded from vesicle lumens and mitochondria (“m” in the axon terminal forming synapse #2). The open arrowhead at the upper left in panel C and detailed in panel A depicts an example of a GAD+ axon process coursing near but not in direct synaptic contact with the cell body. Instead, this process is enveloped by an astrocytic process, depicted with three asterisks in its cytoplasm. The width of the astrocytic process that is inserted between the axon terminal and the cell body is no more than twice the thickness of the plasma membrane, estimated to be approximately 20 nm. For all small panels, except for panel A, the calibration bar equals 600 nm. For panel A, the same bar equals 300 nm. The 2 μ m calibration bar applies to panel C only.

yet we observed a similar increase in running when driving activity in all pyramidal cells, versus the DS-projecting subset, suggesting that the mPFC-DS subset drives the observed effects on FR-evoked running. Thus effects could be mediated by any subset of DS cells projecting to specific downstream targets, as well as collateral projections from mPFC to several additional brain regions, including basolateral amygdala, ventral striatum, and spinal cord (Gabbott et al. 2005). Collateral projections to the ventral striatum are of particular interest, as D2 receptor overexpression in the nucleus accumbens increases FR-evoked

Table 2 Summary of major findings

Condition	Measured parameter	PFC-DS subset	All pyramidal cells
Cell activation; FR	Running	↑	↑
Cell suppression; FR	Running	↓	↓
Cell activation; <i>ad libitum</i> food	Running	0	0
Cell suppression; <i>ad libitum</i> food	Running	0	0
Post mortem	Axo-somatic GABA innervation (EM)	<	
Cell activation; <i>ad libitum</i> food	% GABA-IN expressing c-Fos	>	

Note: List of conditions and the observed effects each produced when applied to either the mPFC-DS subpopulation or the general pyramidal cell population. Rows 1–4 reference Figures 2–3, row 5 references Figure 9; row 6 references Figure 5C. For rows 5 and 6, <and> signs compare the mPFC-DS population versus the general population of pyramidal cells. Up arrow indicates an increase in the measured parameter, down arrow indicates a decrease in the measured parameter, and 0 indicates no difference.

wheel running and reduced food intake to produce precipitous weight loss (Welch et al. 2019).

Axo-Somatic Synaptic Inhibition Preferentially Targets Non-DS-Projecting mPFC Pyramidal Cells

We report here the first evidence that GABA-INs provide less axo-somatic innervation to mPFC-DS-projecting cells, versus neighboring mPFC pyramidal cells that do not project to DS. Axo-somatic inhibition is likely to be from fast-spiking parvalbumin-positive cells (PVs), as this subtype is known for strong axo-somatic inhibition of pyramidal cells (Kawaguchi and Kubota 1997). Fast-spiking PV interneurons preferentially target layer 5 mPFC pyramidal cells with characteristics of PT (pyramidal tract) neurons (thick-tufted apical dendrites, prominent h-current) than of IT (intratelencephalic) neurons (thin-tufted apical dendrites, less prominent h-current) (Lee et al. 2014). Striatum is the only subcortical region that receives both PT and IT projections from layer 5 of cortex (Shepherd 2013). Based on the axo-somatic GABA input pattern, the mPFC-DS subpopulation could potentially overlap more with the IT than with the PT neurons. IT neurons also project preferentially to D1R-expressing striatal cells (Reiner et al. 2010), the latter of which are necessary for FAA (Gallardo et al. 2014). Our data support this notion by revealing that mPFC-DS pyramidal cells also are necessary for FAA.

Axo-Somatic Synaptic Inhibition of Pyramidal Cells as Revealed by EM is Linked to Weight Loss

Individual differences in axo-somatic GABAergic innervation correlates negatively with FR weight loss, suggesting that increased GABAergic innervation may be protective against weight loss. Interestingly, after C21 delivery on FR2, weight loss correlated negatively with GABAergic innervation only to the DREADD-driven mPFC-DS subset of cells responsible for exacerbated FAA, and not to neighboring pyramidal cells. On FR3 and FR4, weight loss negatively correlated best with GABAergic innervation averaged across all layer 5 pyramidal

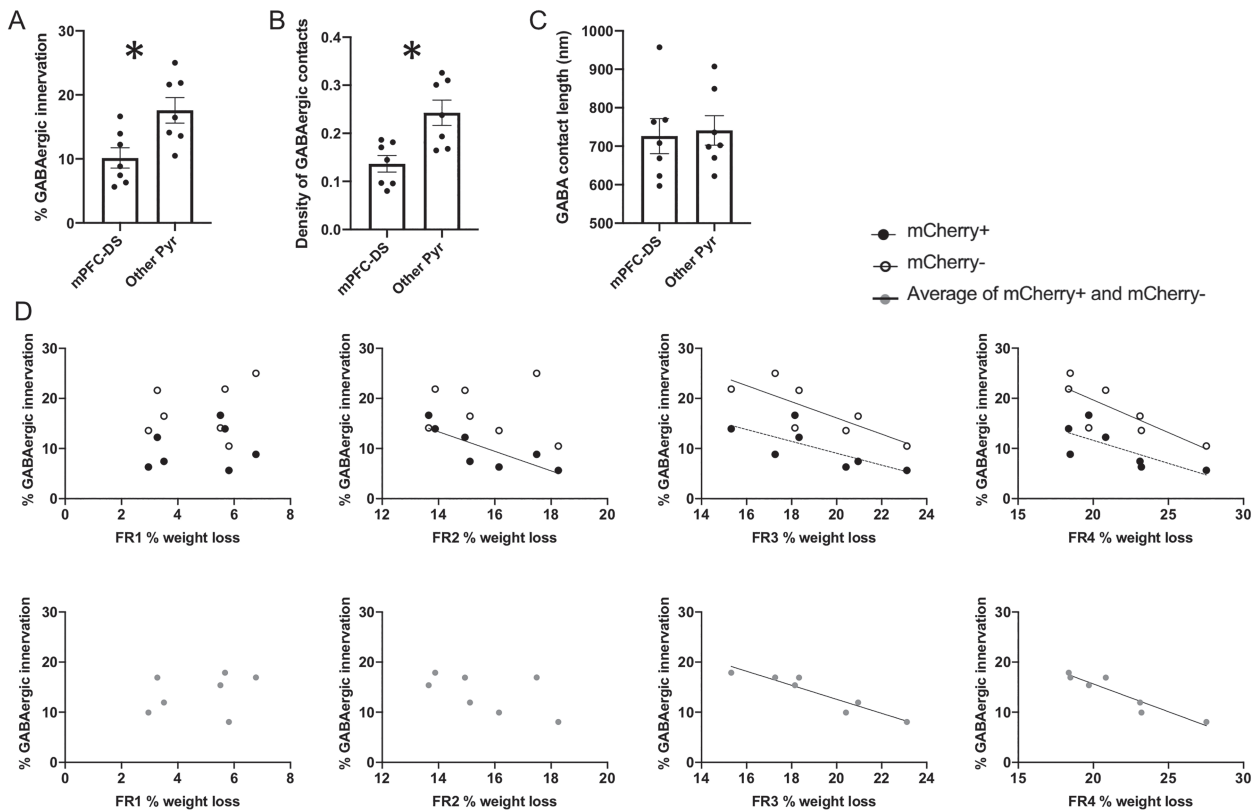


Figure 9. EM analysis of GABAergic innervation of mCherry+ mPFC-DS-projecting neurons and unlabeled neighboring cells in layer 5 mPFC. A–C. mCherry positive pyramidal cells projecting to DS received less axo-somatic GABAergic innervation than neighboring mCherry negative cells, calculated as (A) the percent of the somatic plasma membrane receiving GAD+ terminal contacts. Lower percent GABAergic innervation among DS-projecting pyramidal cells was due to lower density of GABAergic contacts (B), with no difference in GABAergic terminal size (C). Each data point represents the mean value for an individual animal ($N = 7$ subjects), with observation of 10 mCherry+ and 10 mCherry- pyramidal cell profiles per individual. D. Correlations between percent GABAergic innervation and percent weight loss on each of the 4 days of FR. Each data point represents an individual animal. Significant correlations ($P < 0.05$) are indicated with a black line of regression, strong trends ($P < 0.1$) are indicated by dashed lines. Percent weight loss was calculated as the weight at 7 pm on the FR day subtracted from the weight at the start of ABA2, all divided by the weight at the start of ABA2. R- and P-values are listed in text.

cells, indiscriminate of their projection pathway. Correlation of GABAergic inhibition with weight loss as a whole, rather than the parameters of running or food consumption individually, suggests that subjects may have taken different combinations of two strategies (increase consumption and/or reduce wheel running) to minimize weight loss.

Distinction in the Microcircuitry of mPFC Pyramidal Cell Subgroups: DS-Projecting versus Others

Investigation of post mortem c-Fos activity revealed additional characteristics of the mPFC-DS pathway that distinguish this subset from the general mPFC population. Selectively driving the mPFC-DS subset, versus general mPFC pyramidal cell activity, induced a greater percentage of both mPFC pyramidal cells and GABA-INS to become c-Fos positive. Thus, driving mPFC-DS activity produces two seemingly opposed outcomes: increased FAA running (vs. CON subjects) and increased elicitation of GABA-IN activity (vs. CaMKII group). When considered in concert with the EM data described above, a new interpretation emerges: the mPFC-DS pathway recruits more GABA-INS, yet receives less axo-somatic feedback inhibition (Fig. 10). Thus, mPFC circuitry may produce a stop-light effect, whereby mPFC-DS pyramidal cell firing elicits a strong response from GABA-INS which, in

turn, suppresses non-DS-projecting pyramidal cells to a greater extent than the mPFC-DS subgroup. This interpretation is consistent with the observation that C21 elicits $\times 5$ greater c-Fos response from the mPFC-DS pyramidal cells, versus the CaMKII pyramidal cells, generally.

Functional Distinctions of the Pyramidal Cell Groups via Differential Recruitment of GABA-INS

Individual differences in FR-evoked running correlated, not with pyramidal cell c-Fos activity, but instead, with GABAergic response following C21 delivery. For the CaMKII group, C21-driven GABA-IN c-Fos response correlated negatively with running only on FR2, suggesting that individual differences in DREADD-driven GABAergic recruitment accounts for individual differences in running, driven by excitement of those same mPFC pyramidal cells. The negative sign suggests that GABAergic innervation protects against the excessive running that can otherwise become fatal in ABA. Likewise, CaMKII+ pyramidal cell recruitment of GABA-IN, as revealed by c-Fos activity, correlated negatively with weight loss, again suggesting GABA-INS' protective role.

By contrast, individual differences in GABA-IN c-Fos expression elicited by driving the mPFC-DS subset correlated positively

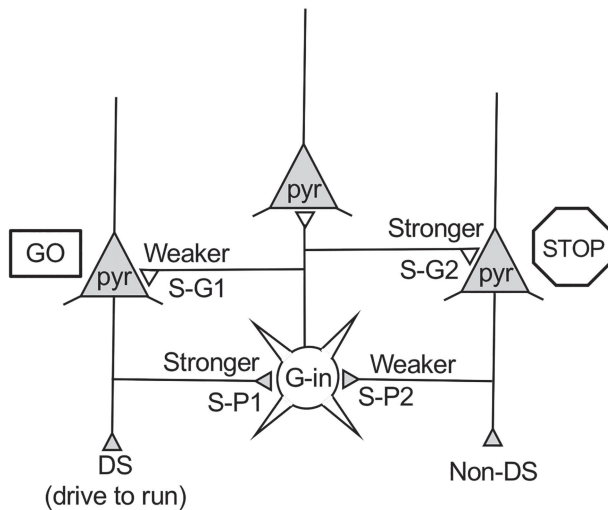


Figure 10. Schematic of mPFC microcircuitry. Pyramidal cells (represented by triangles) that project to DS drive running in the context of FR (Fig. 2A). Widening the population of activated mPFC pyramidal cells to include the non-DS-projecting population does not increase running beyond what is observed by driving the DS-projecting pyramidal neurons (Fig. 3A). mPFC-DS cells elicit a stronger response from GABAergic cells (Fig. 5C, synapse S-P1), which in turn innervate non-DS-projecting pyramidal cells (synapse S-G2) more prevalently than mPFC-DS-projecting pyramidal cells (synapse S-G1, Fig. 9A). This enables the mPFC-DS subgroup to conduct excitatory flow (green light) to elicit FR-evoked running, while suppressing the neighboring non-DS-projecting pyramidal cells. This model is further supported by correlations between individual differences in FR-evoked running and characteristics of GABA-INs, which were revealed by looking separately at GABA-IN-to-Pyr and Pyr-to-GABA-IN relationships. Axo-somatic inhibition of mPFC pyramidal cells (synapses S-G1 and S-G2) correlated with weight retention in general, but not feeding or running in particular, indicating a protective role for GABA-IN suppression of mPFC pyramidal cells through a combined mechanism of enhanced feeding and suppressed running (Fig. 9D). This effect is in keeping with SalB suppression of running, either by targeting mPFC-DS cells or by targeting the general mPFC pyramidal cell population (Fig. 2C and 3C). Likewise, DREADD activation of the general mPFC pyramidal cell population revealed a negative correlation between evoked activity in GABA-INs and evoked running activity, indicating a protective role of GABA-INs in suppressing FR-evoked running (Fig. 5F). By contrast, when DREADD activation was limited to just the mPFC-DS subpopulation that drives hyperactivity, evoked activity in GABA-INs (synapse S-P1) and evoked running activity correlated positively (Fig. 5F), specifically during FR and not during *ad libitum* food availability. Notably, the stop-light interpretation presented here predicts this positive correlation, as greater mPFC-DS activity produces both greater running (DS output) and greater interneuron activity (synapse S-P1), which preferentially targets non-DS-projecting pyramidal cells (synapse S-G2).

with running, specifically during FR and not during *ad libitum* food availability. Both the positive (for the mPFC-DS) and negative (for the CaMKII group) correlations between GABA-IN c-Fos and running support the stop-light interpretation (Fig. 10), where greater inhibitory control of non-DS cells than of the mPFC-DS cells both support running. By this logic, preferential inhibitory axo-somatic target by PV cells onto non-DS cells allows for preferential execution of mPFC-DS dependent tasks—in our case, FR-evoked running. mPFC-DS pyramidal cell firing is necessary for both reward-related cognitive flexibility (Nakayama et al. 2018) and goal-directed action selection (Friedman et al. 2015). Without prior knowledge of the stop-light circuitry revolving GABA-INs, one might expect that mPFC PV cell activation would generally inhibit these mPFC-dependent tasks, but instead, the opposite is reported: PV cell activation

improves goal-directed behavior (Kim et al. 2016) and reward-related cognitive flexibility (Sparta et al. 2014). By contrast, PV cell activation impairs performance on tasks that have not been shown to require the mPFC-DS pathway, as is the case in working memory, social interaction (Ferguson and Gao 2018), and regulation of anxiety (Page et al. 2019). Preferential PV innervation of non-DS-projecting pyramidal cells may explain why PV activation impairs tasks dependent on non-DS-projecting cells, while enhancing mPFC-DS dependent tasks. Notably, the majority of works cited here (Sparta et al. 2014; Kim et al. 2016; Ferguson and Gao 2018; Nakayama et al. 2018) use FR to reduce body weight to ~80–90% of baseline to elicit behavior, which is similar to the percent reduction we observed on FR2. Our findings indicate that FR used in these reward-related cognitive flexibility and goal-directed action selection tasks could have enhanced the engagement of mPFC-DS pathways through increased activation of mPFC PV neurons.

mPFC-DS Pathway in Decision-Making

In the context of severe FR, an organism is presented with the decision to either 1) reduce caloric output (low cost) yet remain in the low-resource region or 2) increase caloric output (high cost) and run to a region that may provide increased resources (potentially high reward). Friedman et al. (2015) found that the mPFC-mDS striosome pathway is necessary for cost-benefit analysis under an approach-avoidance conflict and that chronic stress increased suboptimal high cost/high reward choices via increased excitation of mPFC-driven DS cells (Friedman et al. 2017). Our ABA mice experienced both the chronic stress of single-housing as well as the stress of FR. This environmental stress may likewise have opened the gate for C21 modulation of mPFC-driven DS pathway, tipping the balance toward the high-cost/high-risk decision to run under conditions of low caloric availability. Conversely, closure of the DS gate during the days of *ad libitum* food, free of chronic stress, may explain why C21 could not tip the balance toward the animals' decision to run on days of recovery.

Clinical Relevance

The effect of extreme FR in humans is most extensively studied in the context of AN, a disorder of self-imposed FR. Nearly all subjects with AN exhibit compulsive hyperactivity, which contributes to the severity of the disorder (Sternheim et al. 2015). Every animal model of a psychiatric illness is flawed, and ABA is not an exception. ABA cannot, for example, capture the role of psychological dynamics of AN such as body image distortion or peer pressure to reduce weight (Walsh 2013). ABA and AN do, however, share the hallmarks of food intake reduction, hyperactivity, compulsive behavior, abnormal reward processing, cognitive rigidity, increased anxiety, amenorrhea, and a sensitive period for adolescent onset (Gutierrez 2013; Aoki et al. 2017; Lamanna et al. 2019; Schalla and Stengel 2019).

Receiving less than one federal research dollar per patient, AN is grossly underfunded and poorly understood (Murray et al. 2017). This ignorance leads to stigma and poor treatment availability, each of which contributes to the fact that AN has the highest mortality rate of all psychiatric illnesses outside addiction (Murray et al. 2017). Although public understanding of a biological root for neuropsychiatric illnesses like depression, or even addiction, has improved considerably over recent years,

public understanding of AN remains obscure. This report provides evidence that compulsive, high-risk running typical of AN is the product of FR engagement of specific PFC neural circuits.

In AN, DS is more engaged in making food choices, as compared to healthy controls, and connectivity between mPFC and DS is stronger when subjects choose maladaptive low calorie versus high calorie foods (Foerde et al. 2015), indicating a possible role for the mPFC-DS pathway in AN. GABA_A receptor agonists, used to treat anxiety, are not effective for treating AN, which currently has no FDA approved pharmacological treatment (Frank and Shott 2016). Our data suggest this could be because GABAergic innervation targets primarily non-DS-projecting cells, rather than the mPFC-DS pathway that mediates FR-evoked hyperactivity.

Supplementary Material

Supplementary material is available at *Cerebral Cortex* online.

Funding

The National Institutes of Health (EY13079; F31 MH112372; R25GM097634); the National Science Foundation (DBI-1460880); and New York University (NYU Research Challenge Fund; NYU Dean's Dissertation Fellowship); Vulnerable Brain Project.

Notes

Acknowledgement of assistance: We gratefully acknowledge Ishan Handa, Sabrina George, and Rose Temizer for their role in data collection. We gratefully acknowledge the NYU Office of Veterinary Resource staff and Claudia Farb for their technical support and advice. *Conflict of interest:* None declared.

References

- Anastasiades PG, Boada C, Carter AG. 2019. Cell-type-specific D1 dopamine receptor modulation of projection neurons and interneurons in the prefrontal cortex. *Cereb Cortex*. 29:3224–3242.
- Angeles-Castellanos M, Mendoza J, Escobar C. 2007. Restricted feeding schedules phase shift daily rhythms of c-Fos and protein Per1 immunoreactivity in corticolimbic regions in rats. *Neuroscience*. 144:344–355.
- Aoki C, Chowdhury TG, Wable GS, Chen YW. 2017. Synaptic changes in the hippocampus of adolescent female rodents associated with resilience to anxiety and suppression of food restriction-evoked hyperactivity in an animal model for anorexia nervosa. *Brain Res*. 1654:102–115.
- Carr KD. 2002. Augmentation of drug reward by chronic food restriction: behavioral evidence and underlying mechanisms. *Physiol Behav*. 76:353–364.
- Cassidy RM, Tong Q. 2017. Hunger and satiety gauge reward sensitivity. *Front Endocrinol (Lausanne)*. 8:104.
- Chen X, Choo H, Huang XP, Yang X, Stone O, Roth BL, Jin J. 2015. The first structure-activity relationship studies for designer receptors exclusively activated by designer drugs. *ACS Chem Neurosci*. 6:476–484.
- Chen YW, Actor-Engel H, Aoki C. 2018a. alpha4-GABA_A receptors of hippocampal pyramidal neurons confer protection against activity-based anorexia for adolescent female mice but not for males. *J Cell Mol Neurosci*. 90:33–48.
- Chen YW, Sherpa AD, Aoki C. 2018b. Single injection of ketamine during mid-adolescence promotes long-lasting resilience to activity-based anorexia of female mice by increasing food intake and attenuating hyperactivity as well as anxiety-like behavior. *Int J Eat Disord*. 51:1020–1025.
- Chen YW, Wable GS, Chowdhury TG, Aoki C. 2016. Enlargement of Axo-somatic contacts formed by GAD-Immunoreactive axon terminals onto layer V pyramidal neurons in the medial prefrontal cortex of adolescent female mice is associated with suppression of food restriction-evoked hyperactivity and resilience to activity-based anorexia. *Cereb Cortex*. 26:2574–2589.
- Chowdhury TG, Wable GS, Sabaliauskas NA, Aoki C. 2013. Adolescent female C57BL/6 mice with vulnerability to activity-based anorexia exhibit weak inhibitory input onto hippocampal CA1 pyramidal cells. *Neuroscience*. 241:250–267.
- de Lartigue G, McDougall M. 2019. Dorsal striatum dopamine oscillations: setting the pace of food anticipatory activity. *Acta Physiol (Oxf)*. 225:e13152.
- Ferguson BR, Gao WJ. 2018. Thalamic control of cognition and social behavior via regulation of gamma-aminobutyric acidergic signaling and excitation/inhibition balance in the medial prefrontal cortex. *Biol Psychiatry*. 83:657–669.
- Foerde K, Steinglass JE, Shohamy D, Walsh BT. 2015. Neural mechanisms supporting maladaptive food choices in anorexia nervosa. *Nat Neurosci*. 18:1571–1573.
- Frank GK, Shott ME. 2016. The role of psychotropic medications in the Management of Anorexia Nervosa: rationale. *Evidence Future Prospects CNS Drugs*. 30:419–442.
- Friedman A, Homma D, Bloem B, Gibb LG, Amemori KI, Hu D, Delcasso S, Truong TF, Yang J, Hood AS, et al. 2017. Chronic stress alters Striosome-circuit dynamics, leading to aberrant decision-making. *Cell*. 171:1191, e1128–1205.
- Friedman A, Homma D, Gibb LG, Amemori K, Rubin SJ, Hood AS, Riad MH, Graybiel AM. 2015. A Corticostriatal path targeting Striosomes controls decision-making under conflict. *Cell*. 161:1320–1333.
- Gabbott PL, Warner TA, Jays PR, Salway P, Busby SJ. 2005. Prefrontal cortex in the rat: projections to subcortical autonomic, motor, and limbic centers. *J Comp Neurol*. 492:145–177.
- Gallardo CM, Darvas M, Oviatt M, Chang CH, Michalik M, Huddy TF, Meyer EE, Shuster SA, Aguayo A, Hill EM, et al. 2014. Dopamine receptor 1 neurons in the dorsal striatum regulate food anticipatory circadian activity rhythms in mice. *Elife*. 3:e03781.
- Gelegen C, Collier DA, Campbell IC, Oppelaar H, Kas MJ. 2006. Behavioral, physiological, and molecular differences in response to dietary restriction in three inbred mouse strains. *Am J Physiol Endocrinol Metab*. 291:E574–E581.
- Gerfen CR, Surmeier DJ. 2011. Modulation of striatal projection systems by dopamine. *Annu Rev Neurosci*. 34:441–466.
- Gilman TL, Owens WA, George CM, Metzler L, Vitela M, Ferreira L, Bowman MA, Gould GG, Toney GM, Daws LC. 2019. Age- and sex-specific plasticity in dopamine transporter function revealed by food restriction and exercise in a rat activity-based anorexia paradigm. *J Pharmacol Exp Ther*. 371: 268–277.
- Goltstein PM, Reinert S, Glas A, Bonhoeffer T, Hubener M. 2018. Food and water restriction lead to differential learning behaviors in a head-fixed two-choice visual discrimination task for mice. *PLoS One*. 13:e0204066.
- Gomez JL, Bonaventura J, Lesniak W, Mathews WB, Sysa-Shah P, Rodriguez LA, Ellis RJ, Richie CT, Harvey BK, Dannals RF, et al. 2017. Chemogenetics revealed: DREADD occupancy and activation via converted clozapine. *Science*. 357:503–507.

- Greenwood BN. 2019. The role of dopamine in overcoming aversion with exercise. *Brain Res.* 1713:102–108.
- Gutierrez E. 2013. A rat in the labyrinth of anorexia nervosa: contributions of the activity-based anorexia rodent model to the understanding of anorexia nervosa. *Int J Eat Disord.* 46:289–301.
- Herpertz-Dahlmann B. 2015. Adolescent eating disorders: update on definitions, symptomatology, epidemiology, and comorbidity. *Child Adolesc Psychiatr Clin N Am.* 24:177–196.
- Kanarek RB, D'Anci KE, Jurdak N, Mathes WF. 2009. Running and addiction: precipitated withdrawal in a rat model of activity-based anorexia. *Behav Neurosci.* 123:905–912.
- Kawaguchi Y, Kubota Y. 1997. GABAergic cell subtypes and their synaptic connections in rat frontal cortex. *Cereb Cortex.* 7:476–486.
- Kim H, Ahrlund-Richter S, Wang X, Deisseroth K, Carlen M. 2016. Prefrontal Parvalbumin neurons in control of attention. *Cell.* 164:208–218.
- Lamanna J, Sulpizio S, Ferro M, Martoni R, Abutalebi J, Malgaroli A. 2019. Behavioral assessment of activity-based-anorexia: how cognition can become the drive wheel. *Physiol Behav.* 202:1–7.
- Lee AT, Gee SM, Vogt D, Patel T, Rubenstein JL, Sohal VS. 2014. Pyramidal neurons in prefrontal cortex receive subtype-specific forms of excitation and inhibition. *Neuron.* 81:61–68.
- Marchant NJ, Whitaker LR, Bossert JM, Harvey BK, Hope BT, Kaganovsky K, Adhikary S, Prinszano TE, Vardy E, Roth BL, et al. 2016. Behavioral and physiological effects of a novel kappa-opioid receptor-based DREADD in rats. *Neuropsychopharmacology.* 41:402–409.
- Meijer JH, Robbers Y. 2014. Wheel running in the wild. *Proc Biol Sci R Soc.* 281.
- Mistlberger RE. 2020. Food as circadian time cue for appetitive behavior. <https://doi.org/10.1098/rspb.2014.0210>.
- Murray SB, Pila E, Griffiths S, Le Grange D. 2017. When illness severity and research dollars do not align: are we overlooking eating disorders? *World Psychiatry.* 16:321.
- Nakayama H, Ibanez-Tallon I, Heintz N. 2018. Cell-type-specific contributions of medial prefrontal neurons to flexible Behaviors. *J Neurosci.* 38:4490–4504.
- Narayanan NS, Land BB, Solder JE, Deisseroth K, DiLeone RJ. 2012. Prefrontal D1 dopamine signaling is required for temporal control. *Proc Natl Acad Sci U S A.* 109:20726–20731.
- Page CE, Shepard R, Heslin K, Coutellier L. 2019. Prefrontal parvalbumin cells are sensitive to stress and mediate anxiety-related behaviors in female mice. *Sci Rep.* 9:19772.
- Pati S, Sood A, Mukhopadhyay S, Vaidya VA. 2018. Acute pharmacogenetic activation of medial prefrontal cortex excitatory neurons regulates anxiety-like behaviour. *J Biosci.* 43:85–95.
- Reiner A, Hart NM, Lei W, Deng Y. 2010. Corticostriatal projection neurons - dichotomous types and dichotomous functions. *Front Neuroanat.* 4:142.
- Rothman KJ. 1990. No adjustments are needed for multiple comparisons. *Epidemiology.* 1:43–46.
- Schalla MA, Stengel A. 2019. Activity based anorexia as an animal model for anorexia nervosa—a systematic review. *Front Nutr.* 6:69.
- Shepherd GM. 2013. Corticostriatal connectivity and its role in disease. *Nat Rev Neurosci.* 14:278–291.
- Södersten P, Brodin U, Zandian M, Bergh C. 2019. Eating behavior and the evolutionary perspective on anorexia nervosa. *Front Neurosci.* 13.
- Sparta DR, Hovelso N, Mason AO, Kantak PA, Ung RL, Decot HK, Stuber GD. 2014. Activation of prefrontal cortical parvalbumin interneurons facilitates extinction of reward-seeking behavior. *J Neurosci.* 34:3699–3705.
- Sternheim L, Danner U, Adan R, van Elburg A. 2015. Drive for activity in patients with anorexia nervosa. *Int J Eat Disord.* 48:42–45.
- Stuber GD, Sparta DR, Stamatakis AM, van Leeuwen WA, Hardjoprajitno JE, Cho S, Tye KM, Kempadoo KA, Zhang F, Deisseroth K, et al. 2011. Excitatory transmission from the amygdala to nucleus accumbens facilitates reward seeking. *Nature.* 475:377–380.
- Stuber GD, Wise RA. 2016. Lateral hypothalamic circuits for feeding and reward. *Nat Neurosci.* 19:198–205.
- Thompson KJ, Khajehali L, Bradley SJ, Navarrete JS, Huang XP, Sclocum S, Jin J, Liu J, Xiong Y, Olsen RHJ, et al. 2018. DREADD agonist 21 is an effective agonist for muscarinic-based DREADDs in vitro and in vivo. *ACS Pharmacol Translat Sci.* 1:61–72.
- Valdes JL, Maldonado P, Recabarren M, Fuentes R, Torrealba F. 2006. The infralimbic cortical area commands the behavioral and vegetative arousal during appetitive behavior in the rat. *Eur J Neurosci.* 23:1352–1364.
- Vardy E, Robinson JE, Li C, Olsen RHJ, DiBerto JF, Giguere PM, Sassano FM, Huang XP, Zhu H, Urban DJ, et al. 2015. A new DREADD facilitates the multiplexed Chemogenetic interrogation of behavior. *Neuron.* 86:936–946.
- Wable GS, Min JY, Chen YW, Aoki C. 2015. Anxiety is correlated with running in adolescent female mice undergoing activity-based anorexia. *Behav Neurosci.* 129:170–182.
- Walsh BT. 2013. The enigmatic persistence of anorexia nervosa. *Am J Psychiatry.* 170:477–484.
- Welch AC, Zhang J, Lyu J, McMurray MS, Javitch JA, Kellendonk C, Dulawa SC. 2019. Dopamine D2 receptor overexpression in the nucleus accumbens core induces robust weight loss during scheduled fasting selectively in female mice. *Mol Psychiatry.*
- Wentz E, Gillberg IC, Anckarsater H, Gillberg C, Rastam M. 2009. Adolescent-onset anorexia nervosa: 18-year outcome. *Br J Psychiatry.* 194:168–174.
- White E. 1989. *Cortical circuits: synaptic organization of the cerebral cortex—structure, function, and theory.* Boston: Birkhauser.